

## Article

# Study on Dolomite Thin Layers and Nodules in the Qingshankou Formation Shale Oil Reservoir of Gulong Sag

Guoqing Sun <sup>1</sup>, Wanbai Dong <sup>1</sup>, Xiangguo Zhang <sup>1,\*</sup>, Jianhua Zhong <sup>2,\*</sup> and Ningliang Sun <sup>2</sup> <sup>1</sup> Exploration Enterprise Department of Daqing Oilfield Co., Ltd., Daqing 163453, China<sup>2</sup> School of Resources and Materials, Northeastern University at Qinhuangdao, Qinhuangdao 066004, China

\* Correspondence: zhangxianguo@petrochina.com.cn (X.Z.); zhongjianhuazz@163.com (J.Z.)

**Abstract:** Recently, 15.1 billion tons of shale oil geological resources were discovered in the Qingshankou Formation of Gulong Sag, Songliao Basin, and this discovery has attracted considerable attention. Thus far, the sedimentary environment and diagenetic process of the Qingshankou Formation in Gulong Sag, particularly the reservoir space and accumulation mechanism of the shale oil, are unclear, which has seriously affected the exploration and development of shale oil. Based on detailed core and thin section observation, thin section analysis, mineral analysis, and geochemical analysis, thin layers and concretions of dolostone in Qingshankou Formation shale in Gulong Sag are studied. Three types of layers and nodules can be seen in the core and thin sections: the first is composed of very pure micrite, powdery calcite, or dolomite (dolomite greater than 90%); the second are argillaceous dolomite thin layers or nodules (dolomite content of approximately 75–90%); and the third is a highly impure dolomite thin layer (dolomite content between 50–75%). The chemical composition of three kinds of dolomite thin layers and nodules is different: the contents of CaO and MgO of the pure dolomite thin layer and nodules are more than 40%. The contents of CaO and MgO in the thin layer and nodules of argillaceous dolomite are between 30 and 40%. The content of CaO and MgO in the impure dolomite thin layers and nodules is less than 30%. The reservoir space is developed at the micron or nanometer scale in the thin dolomite layers and nodules, although most of these layers are filled with asphalt. The development of thin layers and nodules of dolomites is related to a dry and hot depositional climate and influenced by hydrothermal fluids. The findings presented here provide important information for exploiting the newly discovered shale oil resources. Many dolostone thin layers and nodules have curved silt veins, and the bending coefficient is 1.48, indicating that the dolostone thin layers and nodules have undergone compaction after formation.

**Keywords:** dolomite; thin layer; nodule; reservoir space; shale oil; Qingshankou Formation; Gulong Sag



**Citation:** Sun, G.; Dong, W.; Zhang, X.; Zhong, J.; Sun, N. Study on Dolomite Thin Layers and Nodules in the Qingshankou Formation Shale Oil Reservoir of Gulong Sag. *Energies* **2023**, *16*, 3981. <https://doi.org/10.3390/en16103981>

Academic Editor: Mofazzal Hossain

Received: 22 March 2023

Revised: 1 May 2023

Accepted: 4 May 2023

Published: 9 May 2023



**Copyright:** © 2023 by the authors. Licensee MDPI, Basel, Switzerland. This article is an open access article distributed under the terms and conditions of the Creative Commons Attribution (CC BY) license (<https://creativecommons.org/licenses/by/4.0/>).

## 1. Introduction

Shale oil is an important oil replacement [1,2] and has recently received a significant amount of attention. Significant progress has been made in shale oil exploration in China, with the following two reservoirs being the most successful examples of exploration and development in China thus far. The first is the Jiyang Depression, whose well Feng1-Ye x has obtained a peak daily production of 260 tons of shale oil and 10,000 cubic meters of shale gas, producing a total of more than 15,000 tons of oil in 200 days. The other is the Erdos West 233 experimental area, where 10 wells were implemented with volume fracturing technology, with an initial average daily production of 13.9 tons of crude oil per well and an average production of 9.6 tons per well at present. The cumulative trial production of six wells has exceeded 10,000 m<sup>3</sup>. By the end of 2016, the cumulative production of crude oil was nearly 200 × 10<sup>4</sup> tons.

Jin Zhijun [1] suggested that, “overall, China is ushering in a shale gas revolution, while the shale oil revolution is yet to come”, indicating that shale oil in China has not

yet reached a market scale. This is explained by the fact that several key scientific issues plaguing shale oil exploration and development have not been resolved, and China is still in the early stages of shale oil discovery [3]. China has huge shale oil resource potential, but its extraction is difficult, and in-depth research is needed concerning the enrichment mechanism, distribution pattern, desert prediction, and low-cost development of land-phase shale oil [3].

The current exploration and development practice shows that the reservoir space, formation mechanism, and reservoir formation law of Gulong's shale oil are extremely different from those of conventional oil and gas reservoirs, and the current mature reservoir formation theories and technologies are unable to overcome these differences. Although great progress has been made in the exploration and development of shale oil in the Gulong Depression Qingshankou Formation, and shale oil wells with a daily production of more than 20–30 tons, such as Gulong Oil Ping 1, have been drilled, producing a total of 10,155.31 tons of oil and 5,412,300 cubic meters of gas, because of the late start, there is still insufficient understanding of certain basic geological problems, thus seriously affecting the speed at which this resource can be used. Therefore, it is important to conduct more research on the basic geology of Gulong's shale oil.

Recently, China has made great progress in the study of shale oil, particularly in the study of lake shale oil, and one of the most important points was the discovery of dolomite in lacustrine shale oil reservoir [4–13]. The physical and chemical properties of the paleoclimate are systematically analyzed. Since the deposition of the third member of the Sha Formation, the warm subtropical climate has gradually become dry, and the water body has gradually become salty, providing the necessary conditions for the formation of dolomite [12].

Many scholars have studied dolomite in the Songliao Basin. Liu et al. [4] was the first to study the dolomite of the Middle Cretaceous Nenjiang Formation in the Songliao Basin and thought that these nodules were formed in the shallow water stage during rapid fluctuations in the lake level. The nodules belong to sedimentary and early diagenetic nodules. Wang et al. [11] also studied the formation mechanism of the Nenjiang Formation dolomite in Well Songke 1 and suggested that the formation mechanism of dolomite is the  $Mg^{2+}$  metasomatism in the Late Cretaceous Songliao Basin caused by marl deposits from turbidite and ostracoda extinction events.

In this study, the following methodologies were used to investigate the thin layers and nodules of dolomite in the shale of Qingshankou Formation in Gulong Sag. The first is core description. We observed the cores of six wells represented by well Guye 8HC, describing in detail and sampling their thin layer dolostone and dolostone nodules. Second, we ground the samples, 350 in total, into thin sheets. Third, we performed mineralogical identification for each sample. Fourth, we selected a typical sample for electron microscope observation based on thin section observation. Finally, we selected typical samples for geochemical analysis.

## 2. Geological Settings

The Songliao Basin is an important hydrocarbon-bearing basin in northern China that covers an area of  $11.95 \times 10^4$  km<sup>2</sup>. It represents a Middle Cenozoic inland fault-collapse superimposed basin that is divided into five primary tectonic units: a central depression, a western slope, a northern dip, a northeast uplift, and a southeast uplift (Figure 1) [14]. The study area is located in the central depression of the primary tectonic unit in the northern part of the Songliao Basin. The main part is located in the Taikang uplift zone and the Longhubo-Da'an terrane, adjacent to the western slope in the west and the Qijia-Gulong Sag in the east; the Longhubo-Da'an terrane represents the main structure [15].

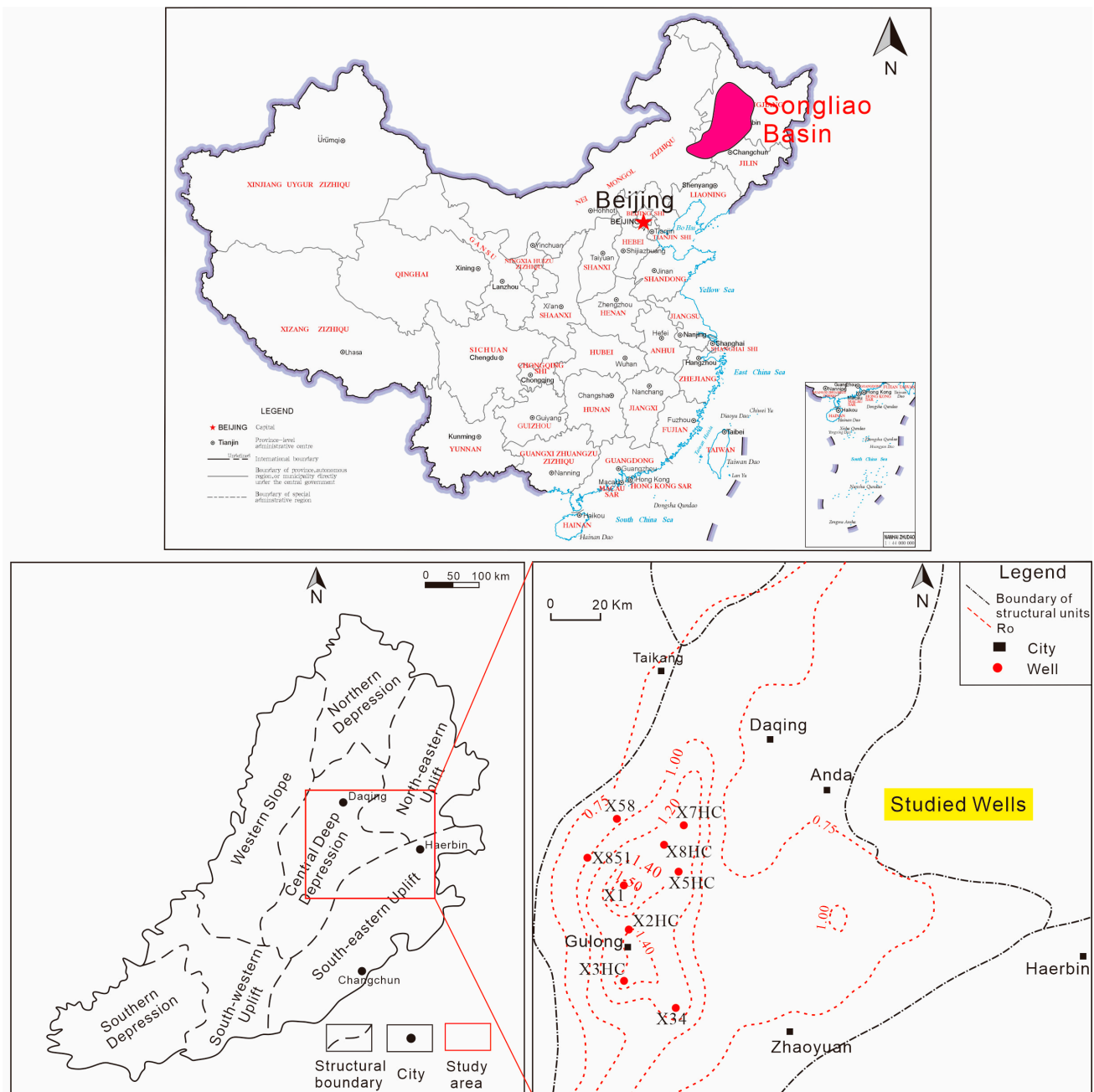


Figure 1. Structural zoning and location of the study area [15].

The sedimentary cover of the Songliao Basin is based on Paleozoic and pre-Paleozoic metamorphic systems and has a maximum thickness of 10,000 m. Moreover, the basin includes the following structures: the Cretaceous Huoshi Ling Formation, the Shahezi Formation, the Yingcheng Formation, the Denglouku Formation, the Quantou Formation, the Qingshankou Formation, the Yaojia Formation, the Nenjiang Formation, the Sifangtai Formation, the Mingshui Formation, and the Cenozoic (Figure 2). The Songliao Basin experienced two large lake intrusions. Gulong Sag, in the central part of the basin, produced a large area of deep and semi-deep lakes, which formed two sets of large-scale lacustrine fine-grained deposits, the Qingshankou and Nenjiang formations, and two sets of high-quality hydrocarbon source rocks, which are the main sources of Gulong’s shale oil. The shale oil of the Qingshankou Formation is a set of black-gray-black mud shales with high organic matter content and three or four oil shale layers at the bottom, and this section developed to contain shale oil [15].

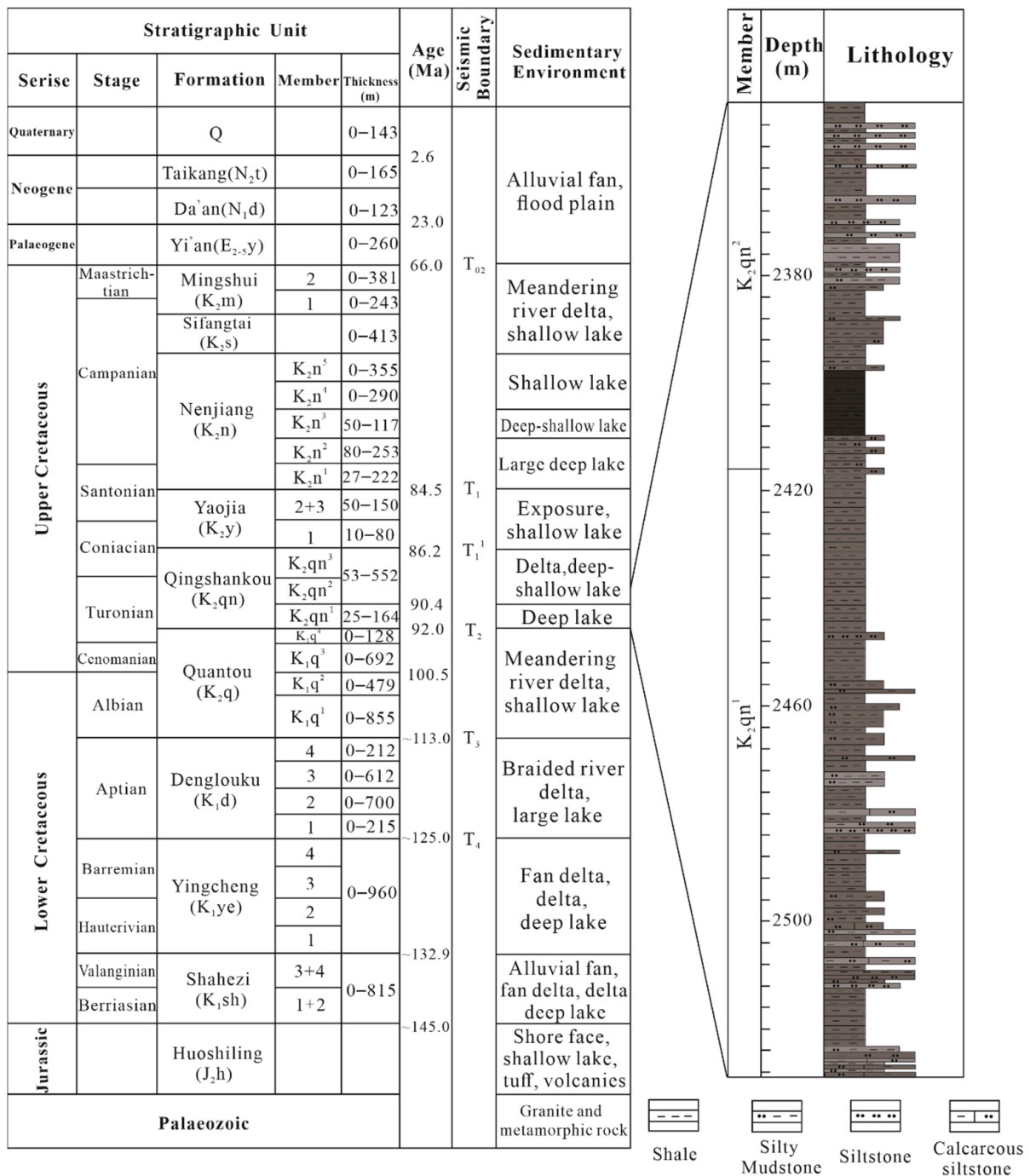


Figure 2. Stratigraphy of the study area [15].

Preliminary exploration and studies have shown that the Qingshankou Formation in the Songliao Basin has developed rich shale oil resources of approximately 15.1 billion tons [3] and is an important replacement resource for the Daqing oilfield. The shale oil source storage ratio of the Qingshankou Formation is greater than 90% [4]. Moreover, the thickness of a single sand body is less than 0.20 m, the cumulative sand body thickness is less than 5% of the entire lithology, and the main shale oil section accounts for less than 1% of the formation; therefore, this formation represents a typical pure shale-type (type iii) shale oil [4]. Many recent studies have focused on the stratigraphy, reservoir characteristics, and shale oil of the Qingshankou Formation [15–23].

The shales of the Shankou Formation in Gulong Sag were formed in a deep and semi-deep lake environment, but were often affected by storms, and typical storm sedimentary

structures and tempestites were developed. Storm deposits are highly useful indicators for facies and paleogeographic analyses [24–28]. Additionally, stormrocks are an important reservoir for stratigraphic traps [25,26,29]. Therefore, studies on tempestites and storm deposits are of great significance. This study introduces and discusses the tempestites and storm deposits recently discovered in the upper Cretaceous Qingshankou Formation in the Gulong Sag of Songliao Basin (Figure 3).

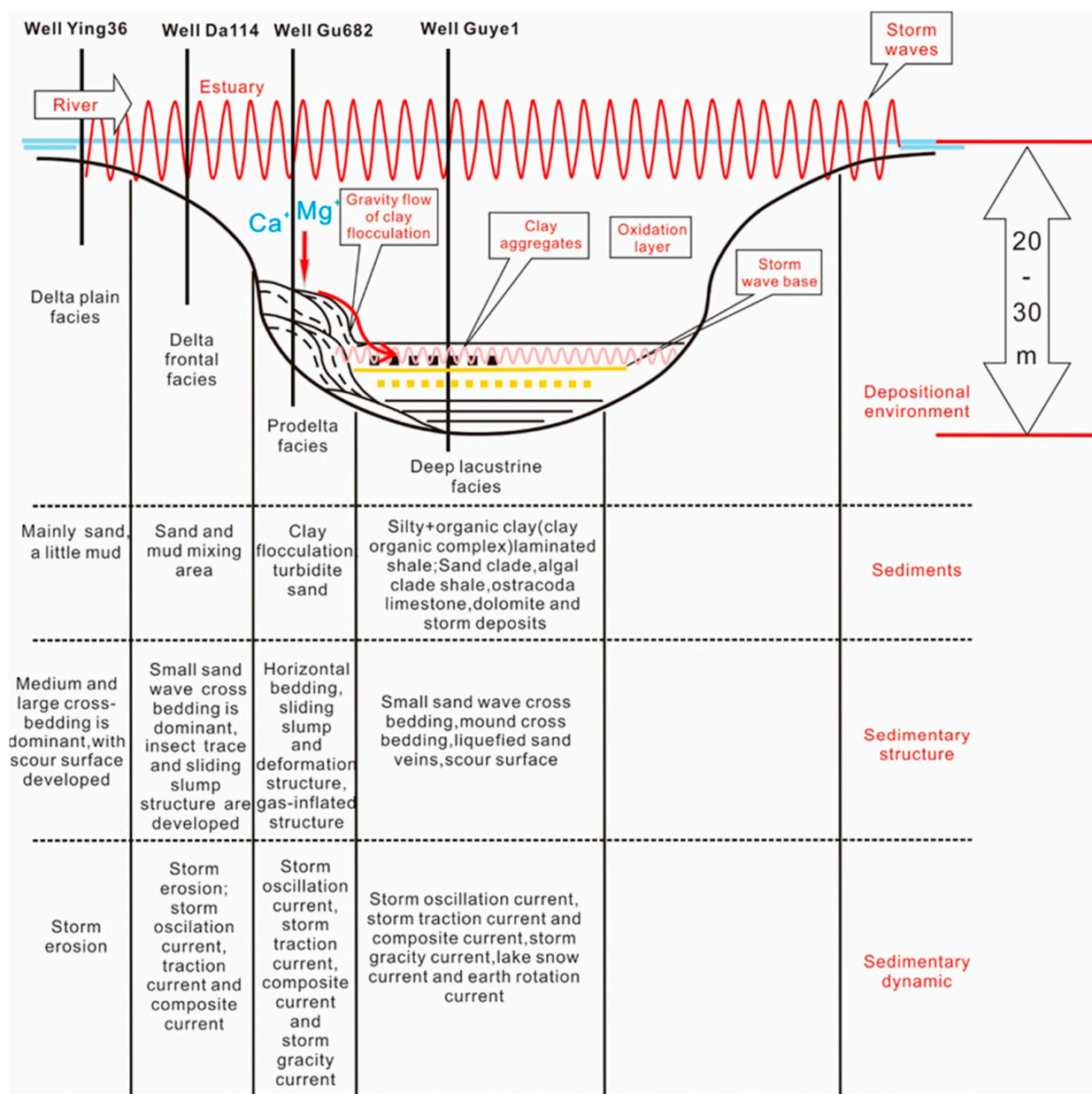
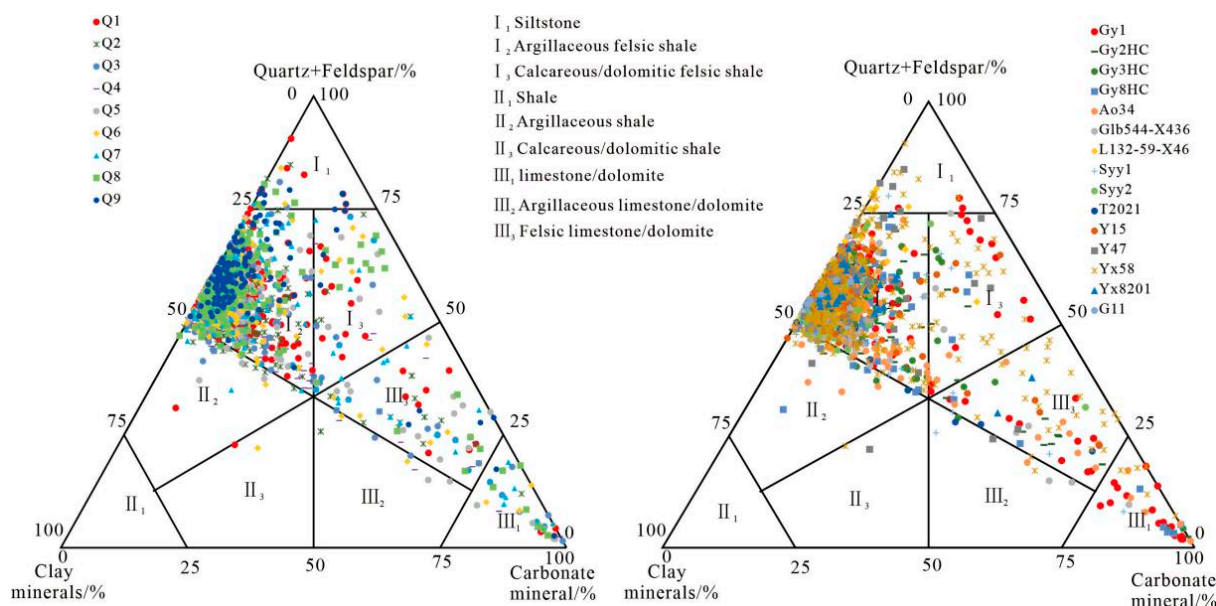


Figure 3. Model of salt lake storm deposition in the Qingshankou Formation, Gulong Sag (after [30]).

Trace element analysis was conducted on several wells in the Gulong Depression (X 8HC, X 3HC, X 58, and other wells) to obtain important information on their paleosalinity and paleoclimate. Taking well Guye 8HC as an example, the geochemical analysis showed that the black shales of the Qingshankou Formation were formed under arid, high-temperature, and humid conditions, with a Sr/Cu above 8.0, reaching 210.12. A Sr/Cu above 10 indicates an arid climate, and as seen in Figure 4, there are more than a dozen extremely arid climates in Qingshankou Q1–Q9, corresponding to 14 Sr/Ba with more than 1 salinization event.



**Figure 4.** Triangulation of the mineral content of the shale oil reservoir in the Qingshankou Formation, Gulong Sag.

### 3. Characteristics of the Gulong Shale Reservoir

#### 3.1. Lithology of the Gulong Shale Oil Reservoir

The Qingshankou Formation in the Songliao Basin consists of a set of fine-grained clastic rocks dominated by shale. In addition to shales, mudstones, liquefied sand–mud mixed rocks, gray-light gray thin-bedded fine sandstones and siltstones, mesomorphic tuffs, yellow-brown dolomites, thin carbonates, and a small number of clouded shales are observed. However, shale is the most important type of sedimentary formation in the Qingshankou Formation.

#### 3.2. Mineral Composition of the Gulong Shale Oil Reservoir

The main mineral composition (above 60%) of the shale oil reservoir in the Gulong Qingshankou Formation is quartz and feldspar. Clay minerals account for approximately 30–40% and include mostly illite, although a small amount of montmorillonite and chlorite are observed. X-ray diffraction (XRD) whole-rock analysis was performed on wells in the reservoir, such as wells Paleo 8HC and Paleo 3HC, and these analyses revealed a mineral composition of quartz ranging from 1.4 to 43.1%, with an average value of 32.9%, and feldspar ranging from 0 to 34.9%, with an average value of 19.5%. The feldspar content was dominated by plagioclase and contained a small amount of potassium feldspar. Carbonate minerals were mainly calcite and iron dolomite, with contents ranging from 0 to 92.7% and an average value of 4.4%, and clay minerals ranging from 0 to 58.8%, with an average value of 35.1%. In general, Cologne shale is a type of felsic clay shale (Figure 4).

The grains of quartz and feldspar are extremely fine, and most of the feldspathic grains are below 0.01 mm or even 0.0039 mm; thus, the rocks show the characteristics of mudstone or shale in structure and are easily classified as clay minerals in thin section. Current outgoing thin section identification results of clay minerals indicate that they account for 80–90% (according to CNPC regulations, 0.0039 mm particles are classified as clay). However, the content of clay minerals is only approximately 30–40%, as identified by XRD based on the chemical and mineral composition of many clay-grade particles. Carbonate rocks account for a small percentage.

### 3.3. Characteristics of Dolomite Thin Layers and Nodules

The thin dolomite layers and nodules examined in this study include thin chert layers and nodules because chert is usually assigned to dolomite. The following is a brief description of the two parts.

#### 3.3.1. Macro-Petrological Characteristics

The thin dolomite layers and nodules in the Qingshankou Formation of the Gulong Sag are grayish, yellowish brown to brownish black (Figure 5) based on the organic matter, clay, and oil contents. The single-layer thicknesses range from centimeters to more than 30 cm, and these layers occasionally appear as dolomite nodules (Figure 5E). Cloudy shale can also be seen (Figure 5E,F), which can also be considered a type of grainy dolomite. Because of the early rock formation time, the strata are harder, stronger, and less deformable and often develop brittle fractures, shear fractures, or friction surfaces; therefore, these layers are often a favorable space for oil and gas accumulation. A number of dolomite thin layers or nodules developed dissolution pores (Figure 5A–C). The dissolution pores were small in size, 1–3 cm in diameter, and contained oil.

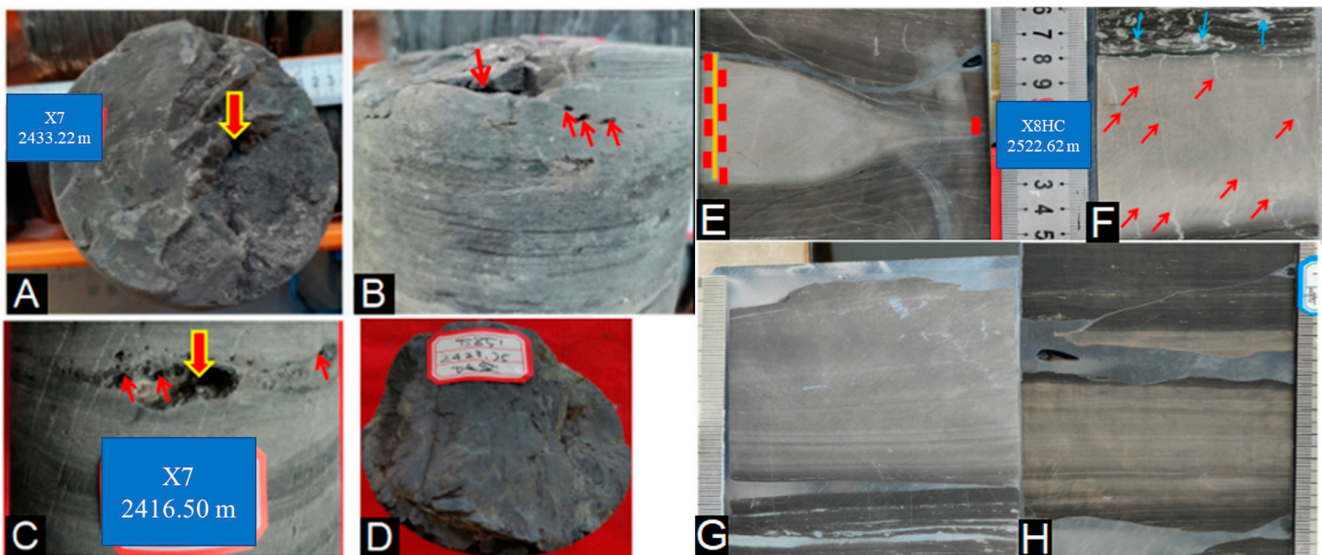


**Figure 5.** Macro-petrographic characteristics of dolomite thin layers and nodules. ((A). Gray-brown dolomite. A dissolution pore seam developed in the middle right and filled with oil (marked by a large red arrow), the height of the label is 2 cm. (B). Grayish-yellow dolomite. Development of fine dissolution pores filled with oil (marked by red arrows). (C). Grayish-yellow dolomite. Development of a fine (small red arrow) and larger dissolution hole (large red arrow) filled with oil, the height of the label is 2 cm. (D). Gray-black dolomite. Developed shear fractures: (E). Dolomite nodules in the form of eyeball turns (red dashed line and yellow line), the height of the label is 2 cm. (F). Numerous liquefied silt veins (red arrows) developed in dolomite nodules (blue arrows). (G). Gray-brown clouded shale developed from the lower phyllite. (H). Yellow-brown clouded shale with phyllite development).

#### 3.3.2. Microscopic Petrographic Characteristics

##### (1) Microscopic features obtained using mobile phones

Direct observations of the cores were performed using an Oppo cell phone microscope, and they revealed that several of the dolomite nodules or thin layers had a large amount of mud flakes (Figure 6). A large amount of chalk-grade mud flakes was observed, and these flakes constituted the skeleton, while dolomite developed as cement between the mud flake particles (Figure 6). Therefore, the contents represented a diagenetic dolomite formed early in diagenesis. The eyeball-shaped dolomite nodule shown in Figure 6B presents star-dotted, sand-grade mud flakes inside and thus represents a clouded sand-flake mudstone nodule. Intact laminae bypass the nodules. The compaction rate can be estimated as approximately

6.0, revealing that the mudstone is strongly compacted. Therefore, compaction should not be neglected when investigating changes in the petrographic phase during rock formation. The genesis of such lenticular mud debris clasts is still worthy of further study, and many more microscopic features will be discussed in a later paper.

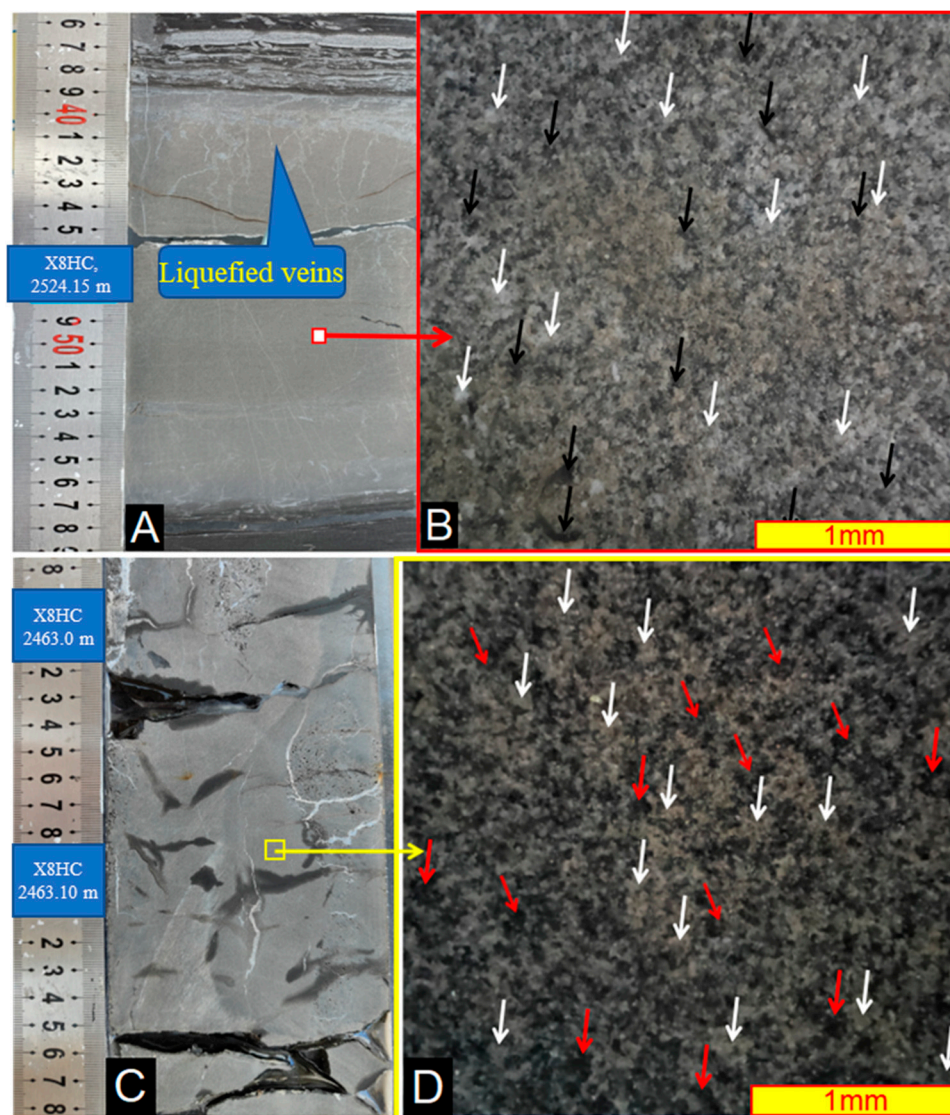


**Figure 6.** Considerable amounts of sand-grade mud debris in argillaceous dolomite. ((A). Oil-bearing dolomite, in which numerous silt veins were developed. (B). Magnification (30 $\times$ ) of the red box in Figure (A) showing dolomite (white arrow) and mud flakes (black arrow). (C). Fractured calcite developed in dolomite. (D). Large number of sand-grade mud flakes (red arrows) and dolomite cementation (white arrows) are visible at 30 $\times$  magnification in the yellow box in Figure (C)).

## (2) Microscopic characteristics

Microscope observations found that the dolomite or calcite content characteristics differed and were divided into three categories:

The first is very pure dolomite (Figure 7A,B), with a mineral composition of 95% dolomite, 1% pyrite, and 4% quartz. The rock has a mud crystal structure that includes mud crystal dolomite crystals, with a small amount of pyrite and chalk-grade debris particles, chalk-grade debris particles in a striped distribution, microfractures filled with brown-black asphaltene, and individual biological debris.

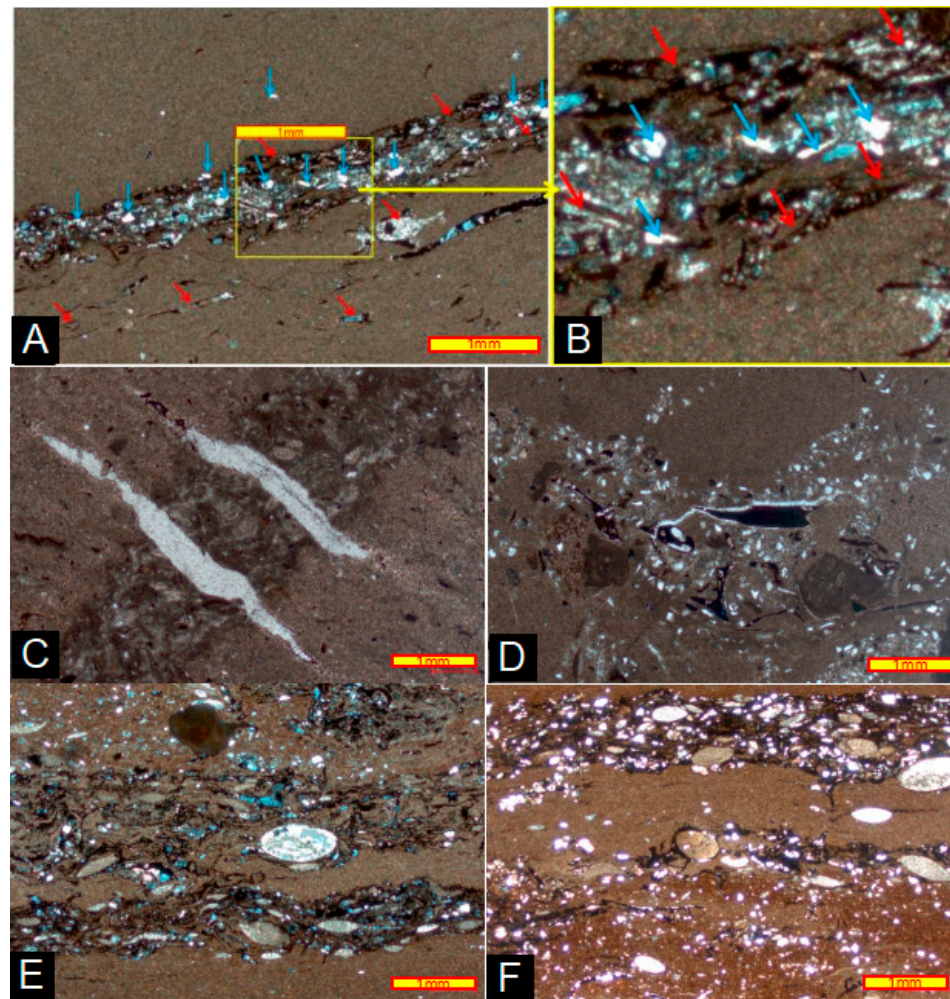


**Figure 7.** Microscopic characteristics of dolomite ((A) very pure dolomite, with a mineral composition of 95% dolomite, 1% pyrite, and 4% quartz; (B) enlargement of the yellow box in Figure (A), clearly showing quartz (blue arrows) and asphalt (red arrows); (C) purer dolomite with ostracodas and other minerals; (D) purer dolomite with felsic minerals; (E) impure dolomite with a great deal of felsic minerals, asphalt, and ostracodas; (F) impure dolomite with a great deal of felsic minerals, asphalt, and ostracodas).

The second was purer dolomite (or chert) (Figure 7C,D) with a mineral composition of calcite (77%), pyrite (3%), quartz (5%), feldspar (2%), rock chips (3%), clay (8%), organic matter (2%), and bioclastic debris (3%). The rock has a powder crystal structure, mainly composed of powder crystal calcite crystals, with brown mud filled between several of the calcite crystals, very fine-grained debris particles in a banded distribution, and pyrite in a patchy distribution. A small amount of brownish-black asphaltene filled the dissolution pores, and a small amount of biological debris was observed in the flakes.

The third type is impure dolomite or cloudy rock (Figure 7E,F) with a mineral composition of calcite (57%), pyrite (4%), quartz (8%), feldspar (5%), rock chips (3%), clay (19%), and organic matter (4%). The rocks were mainly composed of mud, calcite, and pyrite. A small amount of quartz, feldspar, and other land-derived debris particles are seen in a striped sandwich distribution and distributed in a linear and agglomerate form. A small number of raw debris fossils were observed, and the rocks developed in parallel lamination, with interstratified grey mud, iron, and sandy stripes.

### (3) Electron microlithological characteristics

Electron backscatter observations of the thin dolomite layers and nodules of the Qingshankou Formation in the Gulong Sag were performed, and images were obtained

(Figure 8). The dolomite has an automorphic, isogranular rhombic structure; the diameter is 5–10 microns; and the structure is a “fog-centered white rim” (Figure 8C,D). The dolomite crystals are in close contact, or clay developed between the crystals. The intergranular clay developed micropores, which are mostly nacreous (Figure 8) and are often filled with bitumen, indicating their storage capacity. The clay was visually observed to account for 10–20% of the surface area, and it was often coeval with pyrite (Figure 8A). Importantly, intergranular pores developed in the dolomite. Dolomite was often syngenetic with pyrite (Figure 8A–C). Pyrite was either densely packed in patches (Figure 8A) or produced in isolation (Figure 8B,C).

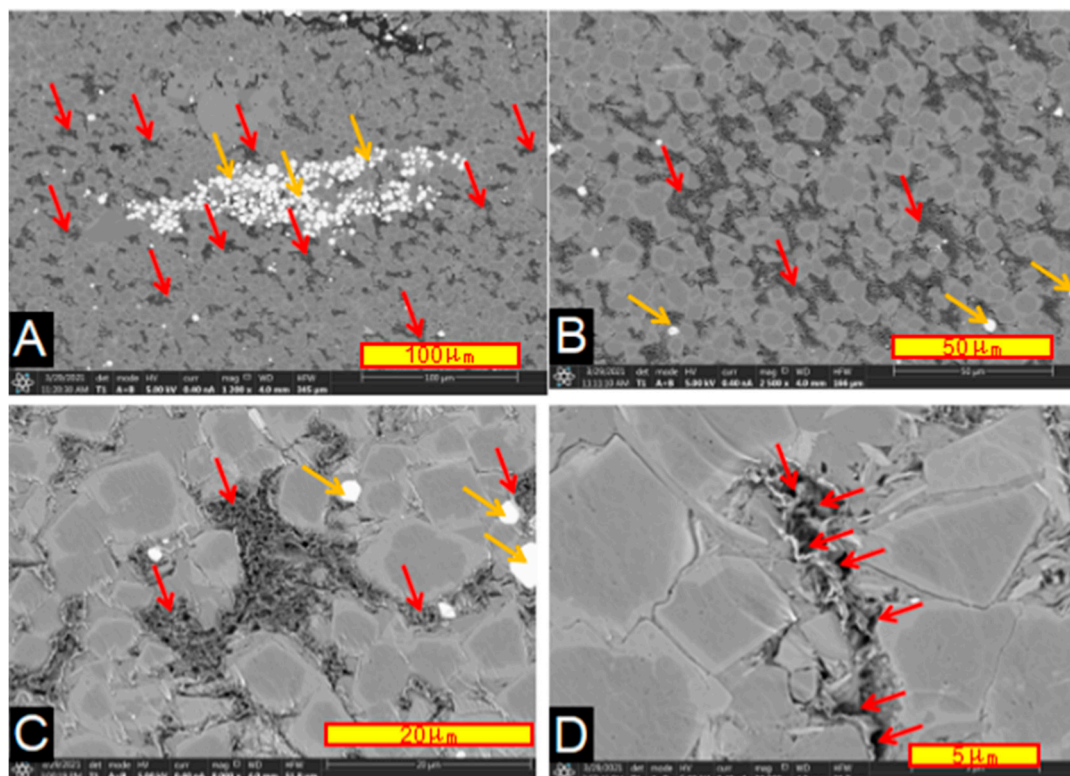


**Figure 8.** Backscattering pattern of dolomite and its intercrystalline nanopores. ((A). Dolomite, pyrite, and green montmorillonite mixed clay; dolomite intergranular pores developed (red arrows); pyrite was produced in aggregates (orange arrows). (B). Illite and chlorite (red arrows) between dolomites; Intergranular pores (red arrows) developed. (C). Dolomite and green monzonite clay (red arrows). Green monzonite clay is sponge-like, in which a large number of nano-pores are developed, which indicates a good storage space, there are some pyrite (orange arrows). (D). Dolomite and green montmorillonite mixed-layer clay (red arrow)).

### 3.4. Mineral Composition of the Thin Dolomite Layer and Nodule

The mineralogical analysis of dolomite thin layers and nodules in the Gulong Qingshankou Formation shows that there are other minerals, such as quartz, feldspar, clay and pyrite, in addition to dolomite (Table 1), fully indicating that the dolomite nodules in Gulong Qingshankou Formation contain impurities, consistent with the results observed under electron microscopy. Based on mineral composition, the thin layer and nodules of dolomite in the Qingshankou Formation in Gulong Depression can be divided into three types: the first is pure white dolomite thin layers and nodules, in which the content of dolomite exceeds 90%; the second is the thin layers and nodules of argillaceous dolomite, in which the content of dolomite is between 75 and 90%; the third is the thin layers and nodules of impure dolomite, and the content of dolomite is between 50% and 75% (Table 1).

**Table 1.** Mineralogical compositions in dolomite thin layers and nodules.

Sample	Depth (m)	Sag	Layer	Lithology	Quartz	Potash Feldspar	Plagioclase Feldspar	Calcite	Ankerite	Clay Mineral	Pyrite	Siderite
A1-4	2484.5	Gulong	K2qn2	Dolomite	1.1	0	1.7	0	94.9	2.3	0	0
A1-5	2486.2	Gulong	K2qn2	Dolomite	3.2	0	1.7	0	92	3.2	0	0
A1-7	2490.5	Gulong	K2qn2	Dolomite	3.2	0	2.5	0	91.2	3	0	0
A1-11	2545.8	Gulong	K2qn1	Dolomite	0.7	0	1.3	0.2	96.6	1.2	0	0
A1-14	2562.6	Gulong	K2qn1	Dolomite	2.8	0	1.3	0	92.4	2.5	1	0
A3-160	2179.8	Gulong	K2qn2	Clay-bearing Dolomite	14.4	0	3	0	78.8	3.8	0	0
A3-171	2189.7	Gulong	K2qn2	Clay-bearing Dolomite	9.4	0	1.8	0	82.4	6.4	0	0
A1-3	2471.5	Gulong	K2qn2	Clay-bearing Dolomite	4.1	0	4.4	0.4	87.5	3.7	0	0
A1-13	2554	Gulong	K2qn1	Clay-bearing Dolomite	10.3	0	1.4	0.4	81	6.9	0	0
A5-2	1596.9	Sanzhao	K2qn1	Clay-bearing Dolomite	3.6	0	2.8	0	86.6	5.8	1.2	0
A4-1	1805.4	Sanzhao	K2qn1	Clay-bearing Dolomite	7.1	0	3.9	0	80	6.2	2.7	0
A3-161	2180.3	Gulong	K2qn2	Argillaceous dolomite	14.7	0	6.2	1.9	64.3	11.1	1.8	0
A3-178	2199.9	Gulong	K2qn2	Argillaceous dolomite	11.5	0	7.1	0	56.7	21.3	2.8	0.7
A3-183	2206.2	Gulong	K2qn2	Argillaceous dolomite	18.7	0	6.9	0	63.6	10.7	0	0
A3-193	2216	Gulong	K2qn2	Argillaceous dolomite	17.1	0	7.3	0	57.5	16.8	1.4	0
A3-243	2256.9	Gulong	K2qn2	Argillaceous dolomite	26.2	0	1.6	0	60.3	10.5	1.4	0
A1-6	2487.2	Gulong	K2qn2	Argillaceous dolomite	8.8	0	4.3	0	76.6	7.5	2.7	0
A1-8	2493.6	Gulong	K2qn2	Argillaceous dolomite	14.6	0	8.7	3.3	60.6	9.8	2.4	0.7
A1-9	2525.2	Gulong	K2qn1	Argillaceous dolomite	6.1	0	3.1	1.1	74.3	12.6	2.7	0
A1-10	2542.8	Gulong	K2qn1	Argillaceous dolomite	7.2	0	2.7	0.9	76.9	10.6	1.7	0
A1-12	2550.4	Gulong	K2qn1	Argillaceous dolomite	14.8	0	2.4	3.5	68.5	10.8	0	0
A1-15	2570.3	Gulong	K2qn1	Argillaceous dolomite	13.5	0	3.2	1.2	69	11.4	1.7	0
A5-1	1593.9	Sanzhao	K2qn1	Argillaceous dolomite	23	0	1.9	0	67.4	7.6	0	0
A5-3	1601.9	Sanzhao	K2qn1	Argillaceous dolomite	15.3	0	8.3	0	60.1	14.2	2.1	0
A5-4	1604.7	Sanzhao	K2qn1	Argillaceous dolomite	11.3	0	3.4	0	75.7	9.5	0	0
A5-5	1636.4	Sanzhao	K2qn1	Argillaceous dolomite	24.5	0	6.6	0	52.1	16.7	0	0
A5-6	1640.3	Sanzhao	K2qn1	Argillaceous dolomite	18.5	0	2.7	0	69.3	9.5	0	0
A4-2	1826.9	Sanzhao	K2qn1	Argillaceous dolomite	15.7	0	3	0	69.7	10.1	1.6	0

### 3.5. Oil-Bearing Properties of Dolomite Thin Layers or Nodules

The dolomite thin layers or nodules were rigid, and shear fractures and calcite veins often developed in the interior. Thin oil-bearing dolomite layers or nodules can often be observed (Figure 9). The storage space of dolomite, as previously discussed, indicates that dolomite develops a certain storage space, and oil or bitumen can be seen in both cores and flakes (Figure 9). Most of the oil in the core developed along the fractures, and a large amount of bitumen could be seen between the crystals of dolomite in addition to the fractures under the microscope. Because the oil is light, it is difficult to observe in the cores and flakes; therefore, only a large amount of bitumen can be seen. Because asphalt fills the pores (Figure 9H), the pore penetration is poor, even when performing physical analysis, affecting its evaluation.

### 3.6. Frictional Mirrors, Abrasions, and Cracks in Thin Dolomite Layers or Nodules

Frictional mirrors or frictional light surfaces, steps, abrasions, and fractures are often observed in thin dolomite layers or nodules that developed on the top and bottom surfaces of the shales of the Qingshankou Formation of the Gulong Sag (Figure 10). The top of the dolomite sometimes has a friction mirror or friction light surface (Figure 10A,B), mainly because the dolomite is hard, and the top (as well as the bottom) surface easily forms a sliding surface in contact with the mud shale during down-layer shearing. Thus, friction mirrors or friction light surfaces are primarily observed. The dolomite top surface step was also a more common structure (Figure 10A–C).

### 3.7. Calcite Veins in Thin Layers or Nodules of Dolomite

Calcite veins are often observed in thin dolomite layers or nodules in the shales of the Qingshankou Formation in the Gulong Sag (Figure 11). Calcite veins are mostly irregular and tilted at various angles in the thin dolomite layers or nodules (calcite veins in mud shales are mostly upright or horizontal). Their widths also varied widely, reaching up to 1 cm. Most veins contain oil and are yellow-brown in color. The oil smell is strong after breaking them open, indicating that the calcite veins have a certain storage capacity. Calcite veins in the mud shale have been dated to 76–24 Ma, which corresponds to a period between the end of Neng and Yi'an and, thus, may be related to reservoir formation. Under the microscope, calcite veins can be seen in microscopic or short columnar form, and they “grow” outward along a central vein, revealing that the calcite veins were “growing” during continuous fracture expansion.

### 3.8. Sand-Grade Mud Flakes in Thin Argillaceous Dolomite Layers and Nodules

The thin argillaceous dolomite layers and nodules in the shales of the Qingshankou Formation in Gulong Sag have a large amount of sand-grade mud flakes (Figure 12), with grain sizes of fine chalk and fine sand in the range of a few percent to 50% (Figure 12), which is extremely poor, and rounding is not observed (Figure 12B). The mud flotsam is endoclastic and formed by bottom currents caused by storms, turbidity currents, and Koch currents tearing apart the originally deposited mud transport, which underwent dolomitization soon after deposition, thus forming thin layers of dolomite and dolomite nodules.

### 3.9. Dolomite Storage Properties

Core observations show that certain dolomites contain not only fractures and calcite veins but also oil, indicating that these dolomites have storage capacity. Observations of dolomite flakes also indicate that several dolomites had dissolution pores (Figure 12); the micropores were more developed but largely filled with bitumen (Figure 13A); and only a few pores were filled with cast gel (Figure 13B). Because the pores are filled with bitumen, the porosity and permeability are greatly reduced when the pore space is measured at the surface; therefore, the dolomite may be considered poorly permeable. However, this is not the case under subsurface overburden conditions. The pore seepage of dolomite must be

further investigated, although the small proportion of dolomite in the entire Qingshankou Formation shale indicates that an accurate evaluation of its pore seepage is inconsequential.

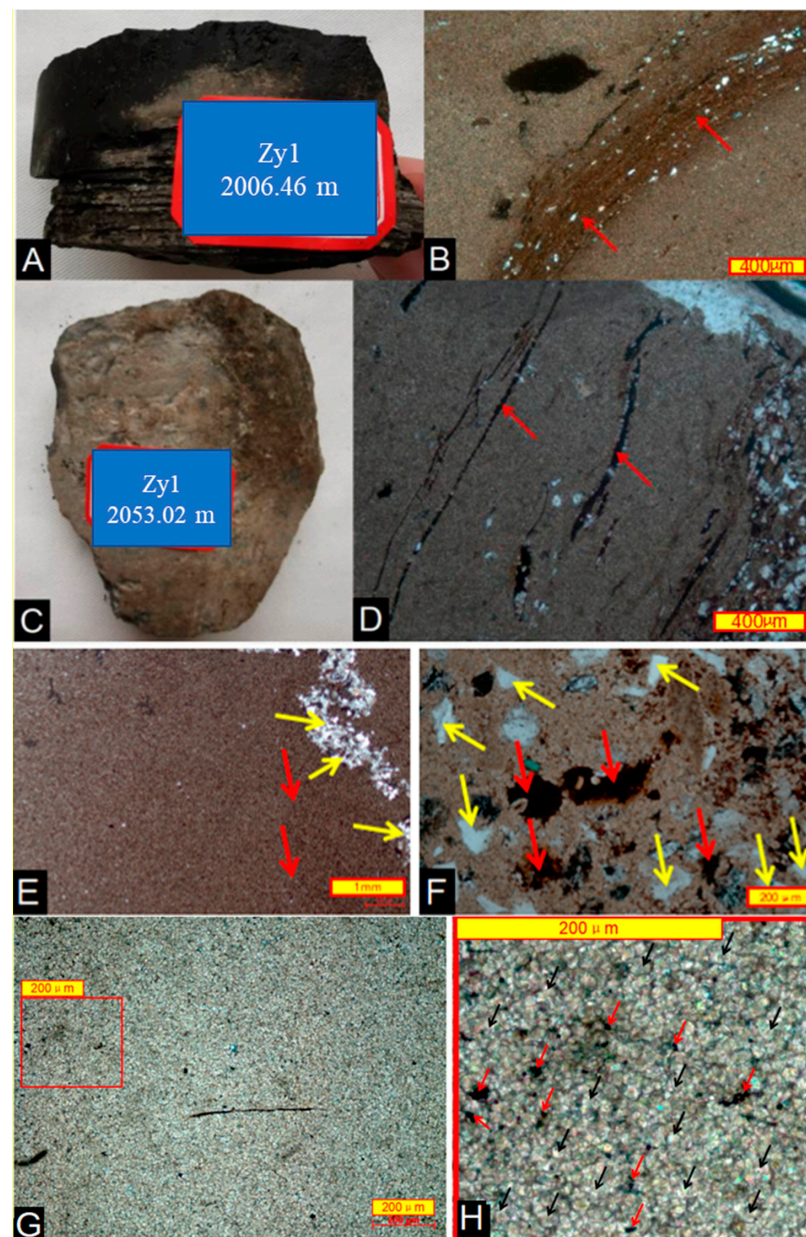


**Figure 9.** Oil-bearing dolomites. ((A). An oil-saturated dolomite nodule, the height of the label is 2 cm. (B). Micrograph of Figure (A) showing that it is mainly a fine-grained dolomite with a microshear strip (red arrows) in the middle containing felsic minerals and there are bitumen strips and bitumen clumps. (C). Oil-bearing dolostone nodule, the height of the label is 2 cm. (D). Micrograph of Figure (C) showing that it is mainly a fine-grained dolomite containing felsic minerals at the right bottom, as well as bitumen strips (red arrows) and bitumen clumps. (E). Micrograph of Figure (C) showing that it is mainly a fine-grained dolomite (red arrows) containing felsic minerals (yellow arrows) at the upper right corner, which appears to be a suture line. (F). Micrograph of Figure (C) showing a significant amount of bitumen (red arrows) and felsic minerals (yellow arrows). (G). Uniform fine-grained dolomite with intergranular pores filled with bitumen. (H). Enlarged view of the red box in Figure (G) showing that the intergranular pores are filled with bitumen (red arrows), and they are scattered among the dolomites (black arrows)).

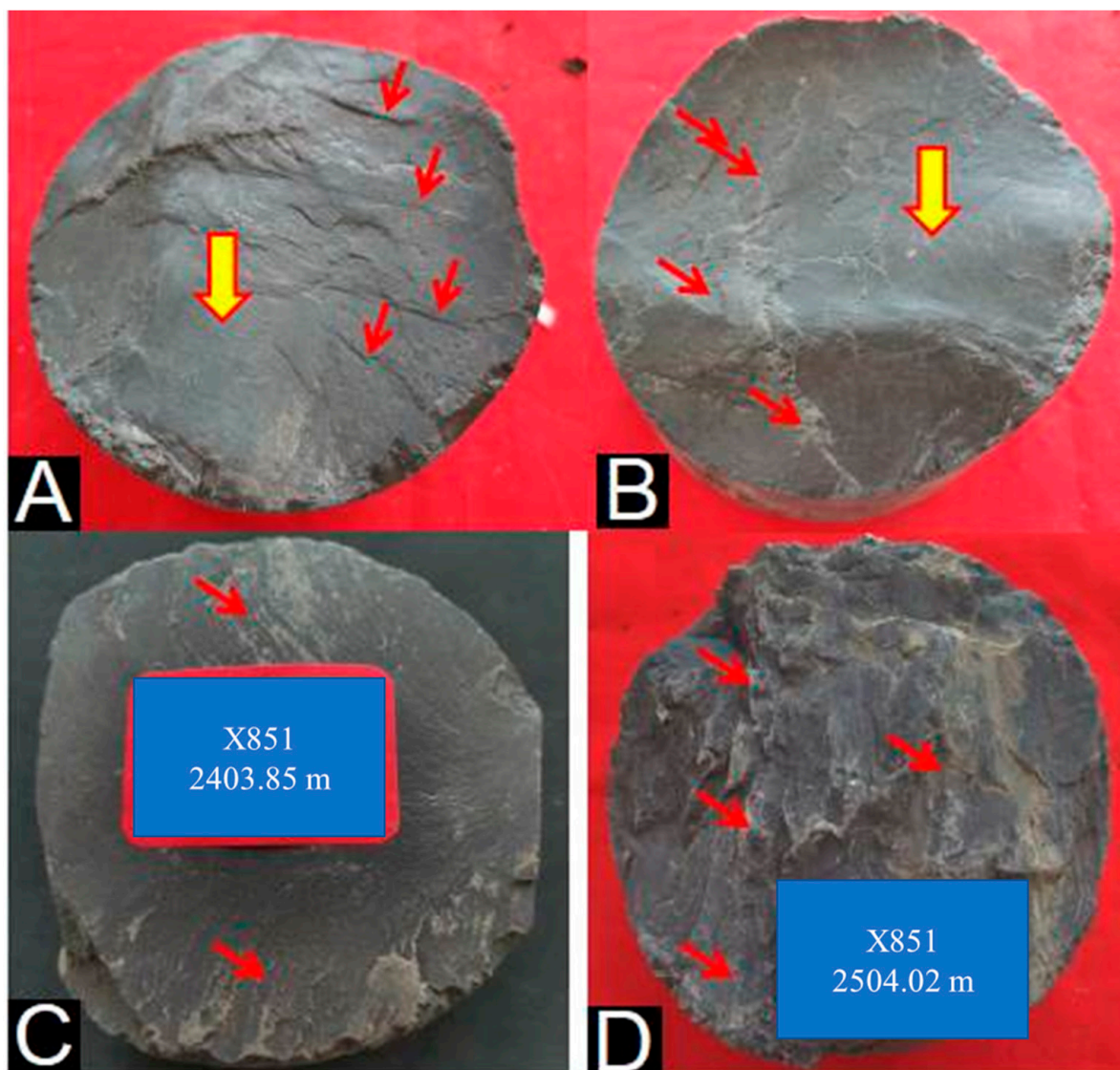


**Figure 10.** Friction surface and step on the top surface of dolomite. ((A). Frictional light surface (large yellow arrow) and steps (red arrow) of the dolomite top surface. (B). Frictional light surface (large yellow arrow) and step (red arrow) of the dolomite top surface. A frictional luminous surface in the form of waves and the direction of the step, with waves in the form of a step. (C). Flattened shear surfaces on which steps developed (red arrows), the height of the label is 2 cm. (D). Dense cracks (red arrows) on the top surface of dolomite, the height of the label is 2 cm).

### 3.10. Carbonized Biological Residues in Dolomite

Carbonized organisms are often observed in dolomite (Figure 14), most of which are likely plants with clearly visible remnant cells (Figure 14A–C). The carbonized organism in Figure 14A is tripod-shaped, with two well-preserved cells (yellow arrows) on the lower edge, thus revealing that it is a carbonized plant remnant. Figure 14 shows a carbonized plant with developed cells and dense cellular cavities (yellow cells) visible inside. Figure 14C shows a bifurcated carbonized plant remnant (perhaps an animal bone fragment). Such contents are relatively common. Figure 14D shows carbonized plant remnants that developed residual cellular structures. Figure 14E shows a circular carbonized plant remnant that may represent a unique cross-section. Figure 14F shows half of the carbonized ring with an apparent internal residual cell cavity. The carbonized organism in Figure 14G is larger and appears to have an internal longitudinal cellular structure, and the perimeter dolomitization is stronger (yellow arrows), revealing that

dolomitization may be related to organic matter. The mineral composition of this dolomite was calcite (83%), quartz (3%), pyrite (2%), clay (4%), and organic matter (2%). The presence of carbonated organic matter in dolomite reveals that the genesis of dolomite is related to these carbonated plants.

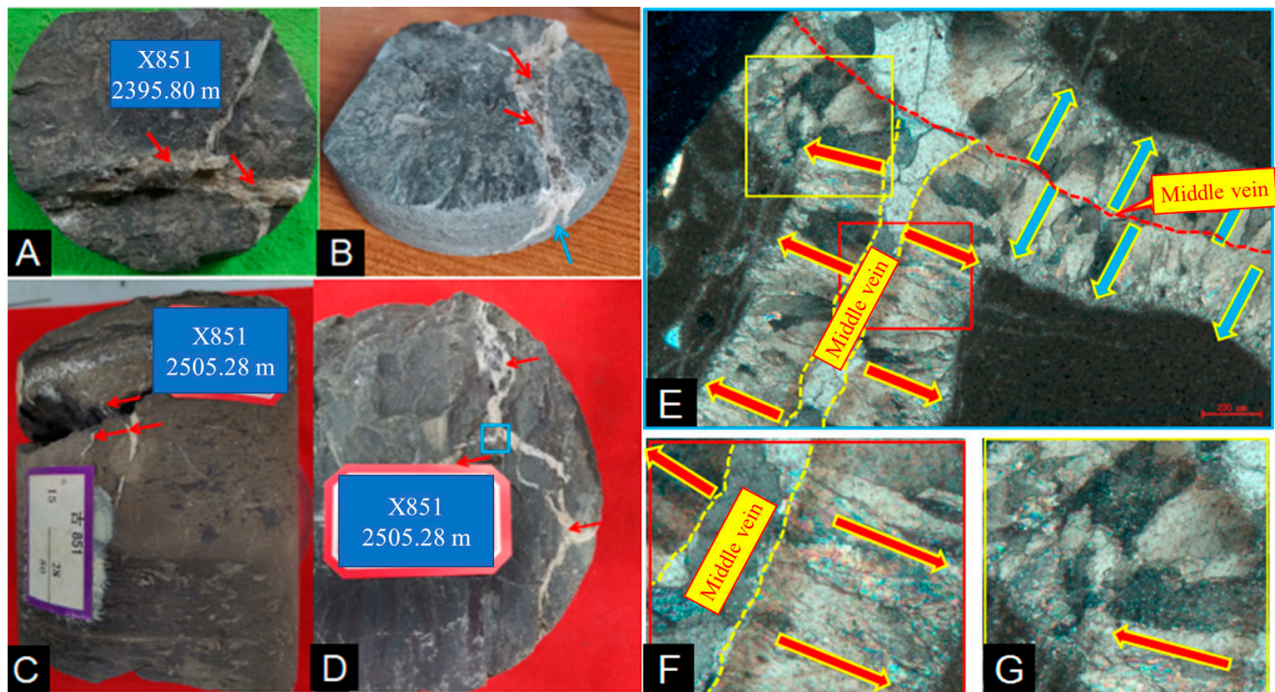


**Figure 11.** Calcite veins in dolomite. ((A). Calcite veins in dolomite, irregular; calcite veins yellowish-brown with oil (red arrows); tensor vein, the height of the label is 2 cm. (B). Three-dimensional view of panel (A). Calcite veins bifurcating acutely downward (blue arrows); calcite veins yellowish brown and contain oil (red arrows). (C). Calcite veins (red arrows) in dolomite, irregular, downward-pointed extinction, tensor veins, the height of the label is 2 cm. (D). Calcite veins (red arrows) in dolomite and irregular and strongly divergent tensor veins, the height of the label is 2 cm. (E). Magnification of the blue box in Figure (D) showing the calcite veins growing direction (red and blue arrows) along a thinner midvein, nearly symmetrical on both sides. (F). Magnification of the red box in Figure (E) showing that calcite veins are composed of finer calcite crystals. The red arrow indicates the direction of calcite crystal growth. (G). Magnification of the yellow box in Figure (E) showing that calcite veins are also composed of finer calcite crystals (red arrow).).

### 3.11. Study of Silt Veins in Argillaceous Dolomite and Their Compaction Rates

Many dolomite thin beds and nodules have developed silt veins (Figure 15). The silt veins in dolomite (nodules) have the following characteristics: (1) They are occasionally developed with silt veins, which are less common than those in dark gray mud shale. (2) The silt veins are slender, mostly 1–2 mm in width and several centimeters in height. (3) The silt veins are mostly straight or slightly curved, with small curvatures. This curvature is significantly higher than the curvature of the silt veins in the dolomite, indicating that the compaction rate of the dolomite thin layer was smaller than that of the mudstone. In addition, the curvature of silt veins in dolomite veins can also reflect the formation time of dolomite during early diagenesis. (4) Most of the dolomite contains a large amount of gray-black sand-grade mud flakes; therefore, most of the dolomite is clouded mudstone or clouded shale. (5) The silt veins in the dolomite were all upright or suberect, indicating that they did not undergo bedding foliation shear as they did in the mud shale, revealing that the dolomite was already hardened when the cis-layer shear occurred.

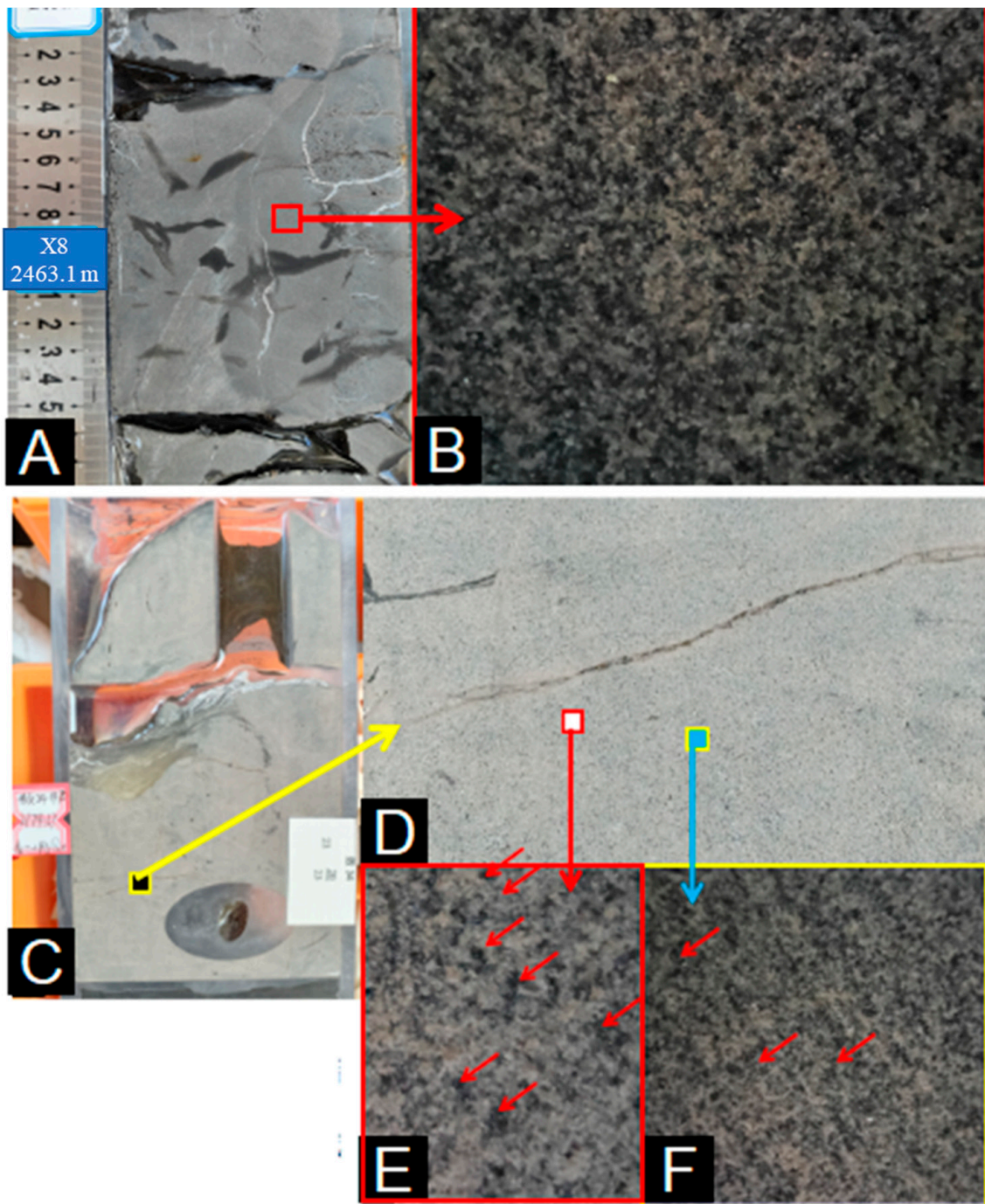


**Figure 12.** Argillaceous dolomite and its microscopic characteristics. ((A). Argillaceous dolomite nodules developed with fractures and calcite veins. (B). Enlarged view of the red box in Figure (A). It is formed by a large amount of gray-black silty silt and dolomite cement. (C). Another dolostone concretion. (D). Enlarged view of the yellow box in Figure (C). Large quantities of silty silt and dolomite cement between the silt are also observed. (E). Enlarged view of the red box in Figure (D). Large quantities of silty mud particle (red arrows) and dolomite cement between mud particles are also observed. (F). Enlarged view of the yellow box in Figure (D). Large quantities of silty mud particles (red arrows) and dolomite cement between mud particles are also observed).

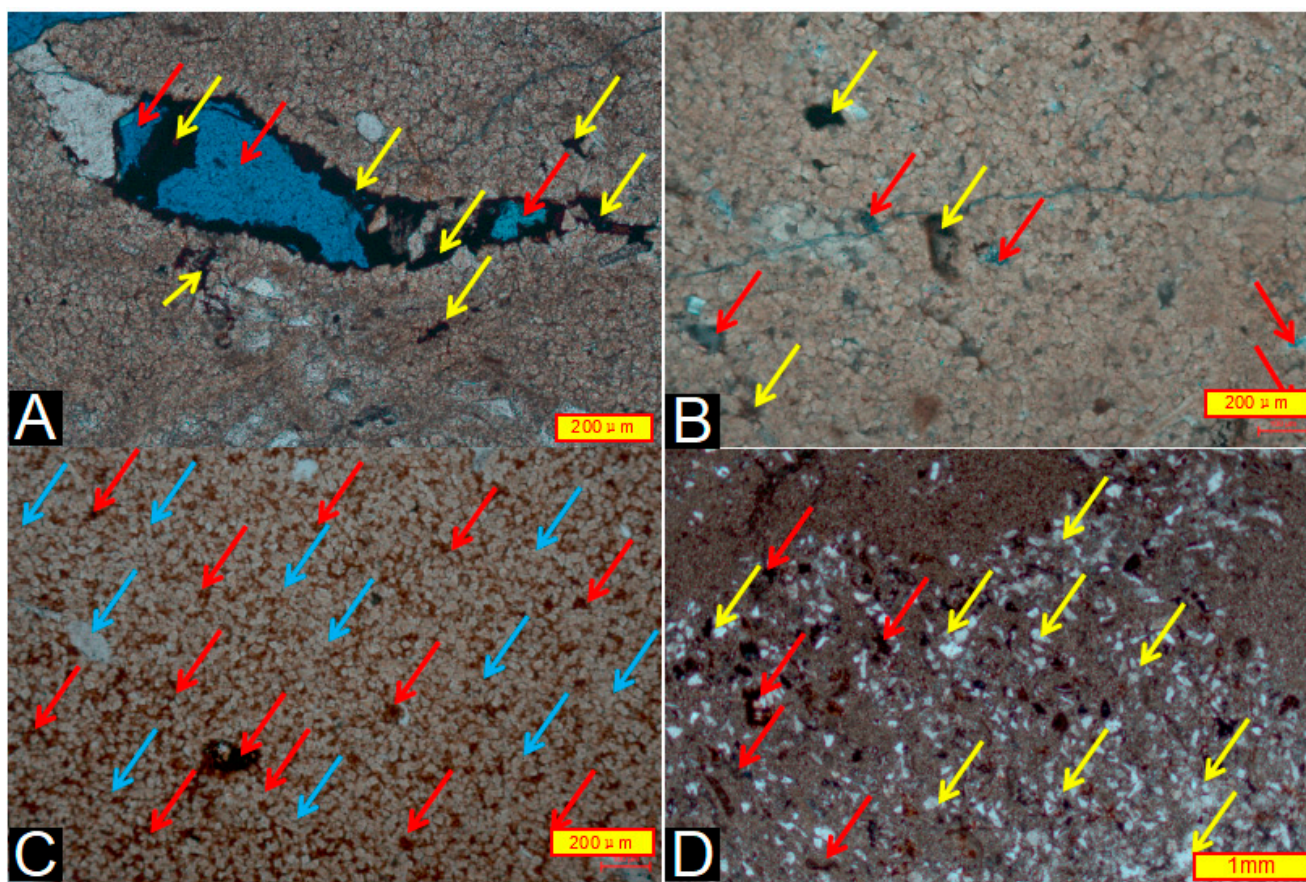


**Figure 13.** Reservoir space of clay-bearing dolomite. ((A). Dissolved pores (red arrows) partially filled with bitumen (yellow arrows). (B). Large number of weak dissolution pores developed between dolomite grains, which are filled with casting gel (red arrows) and bitumen (yellow arrows). (C). Great number of pores filled with bitumen (red arrows) between dolomite grains (blue arrows). (D). A significant number of felsic particles (yellow arrows) mixed locally and bitumen (red arrows) that occupy the dissolved pores).

The curvature of the silt veins in the dolomite thin layers and nodules is small, and quantitative studies of the silt veins in the dolomite thin layers (red) and silt veins in the mud shale above the dolomite thin layers (blue) in Figure 16 were performed to obtain certain parameters, as summarized in Table 1. The average curvature of the silt veins (red) has a value of 1.48 (Table 2), while the curvature of the silt veins in the mud shale above the dolomite thin beds (blue) can reach 2.68 (Table 3). A large amount of black mud flakes (yellow arrows in Figure 16B) can be seen under  $30\times$  magnification of the dolomite thin layer, and the content of mud flakes is approximately 40–50% according to visual inspection. The compaction of dolomite may primarily be related to the compaction of clay chips. The curvature of silt veins in mud shales reached a value of 5.0–6.0 [15]. Curvature studies of silt veins in dolomite thin-layered chalk nodules revealed that the compaction rate of the dolomite thin layers and nodules is significantly lower than that of the mud shale at the same depth, suggesting that dolomitization occurred soon after deposition or during early diagenesis.

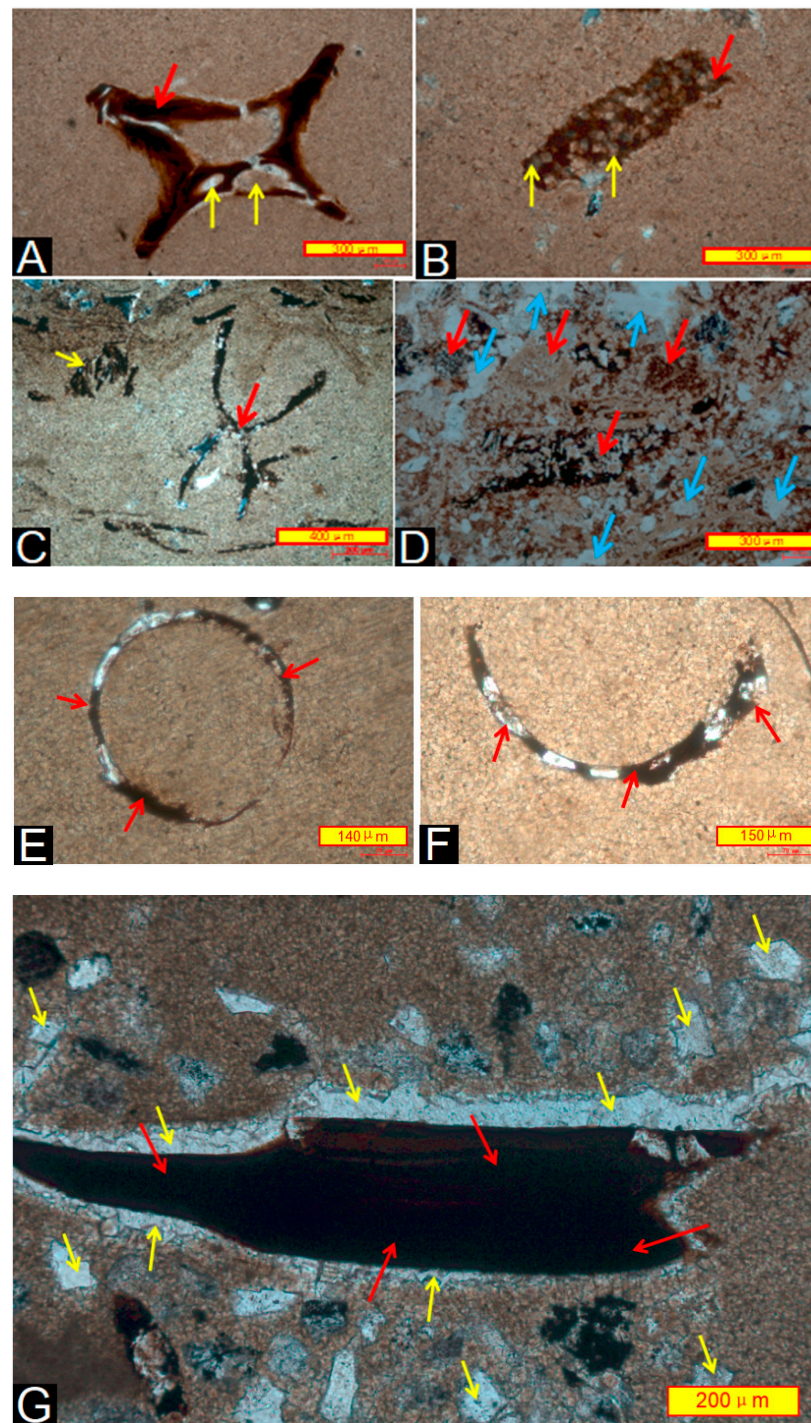


**Figure 14.** Suspected carbonized biofossils in dolomite. ((A,B). Organisms with cellular structure (red arrows) containing two well-preserved cellular lumens (yellow arrows). (C). Double-aeolian organic matter (red arrows) with a large amount of residual cellular cavities (yellow arrows). The black color is due to intense carbonation. (D). Organic matter with cellular structure (red arrows), and a large number of long particles (blue arrows). (E). Circled carbonized plant residue (red arrows), produced in pure dolomite. (F). Semicircular rings of carbonized plant residues suspected (red arrows) to be produced in pure dolomite. (G). Large carbonized plant remnant (red arrow) with strong dolomitization on the outer rim and transformation from mud crystal calcite to larger dolomite crystals (yellow arrow)).

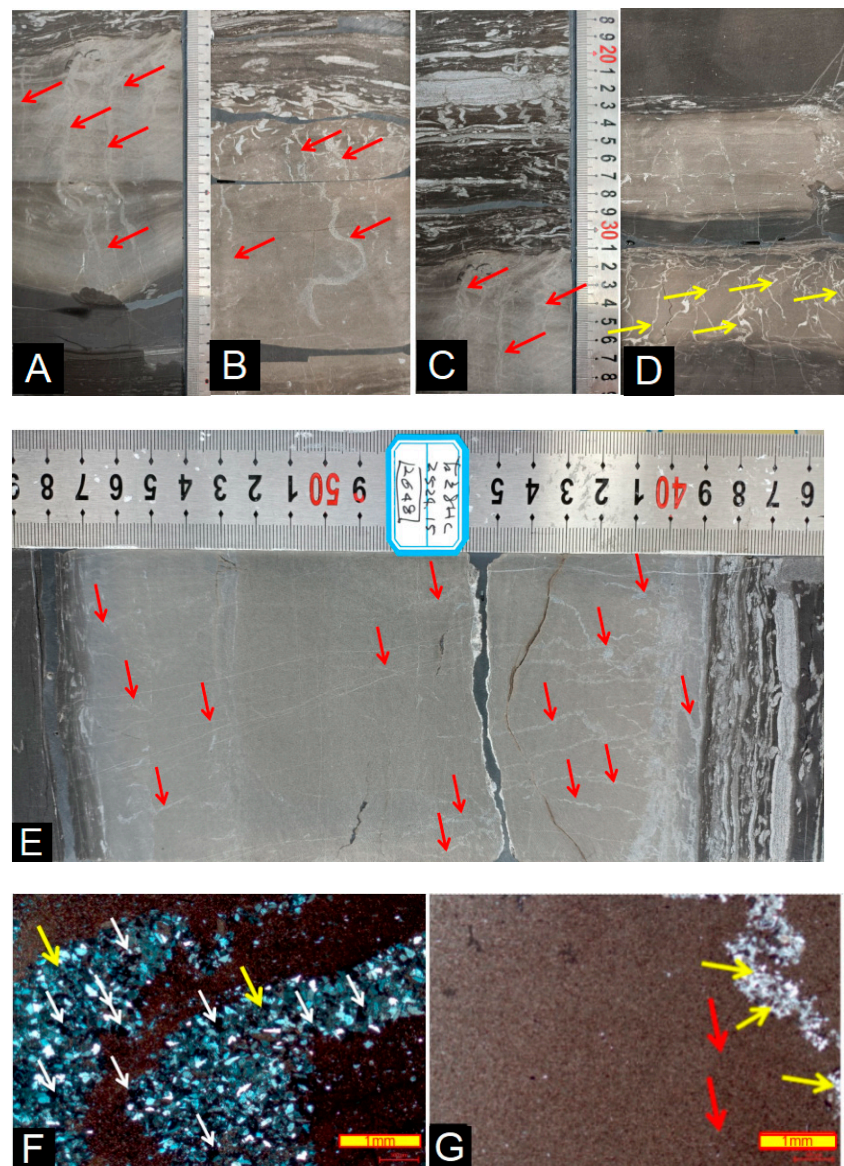


**Figure 15.** Silt and calcite veins in thin layers of clay-bearing dolomite and nodules. ((A). Development of slightly curved silt veins (red arrows) in the dolomite reveals that consolidation of the dolomite occurred early in diagenesis and that little compaction occurred during later diagenesis. (B). Complex silt veins (red arrows) developed in the dolomite; the upper veins are small in size but complex, and one silt vein in the middle is more bent and “S”-shaped, although the bending rate is smaller than that of the silt veins in the clay. (C). Complex silt veins (red arrows) developed in the dolomite, and they are complex in the upper part, simple in the middle and lower parts, and linear. This indicates the absence of compaction shortening in the vertical direction. (D). Complex silt veins (yellow arrows), with the lower ones calcified. The silt veins in the upper dolomite layer were flatter and straighter, indicating that they were not bent by compaction. (E). Large number of penetrating silt veins (red arrows) developed in the thicker dolomite, and the top was denser and more complex. The middle and lower parts were simpler and had less curvature, indicating less compaction. (F). Micrograph of a silt vein in dolomite, coarser and curved; a large number of mud flakes (white and yellow arrows) are visible, revealing that the silt vein passed through the mud into dolomite. Orthogonal polarization is observed. (G). Micrograph of a silt vein (yellow arrow) in dolomite, more slender and curved, like intestines. There are great deals of bitumen (red arrows) between dolomite. This is the same photo as Figure 9E. Orthogonal polarization is observed).

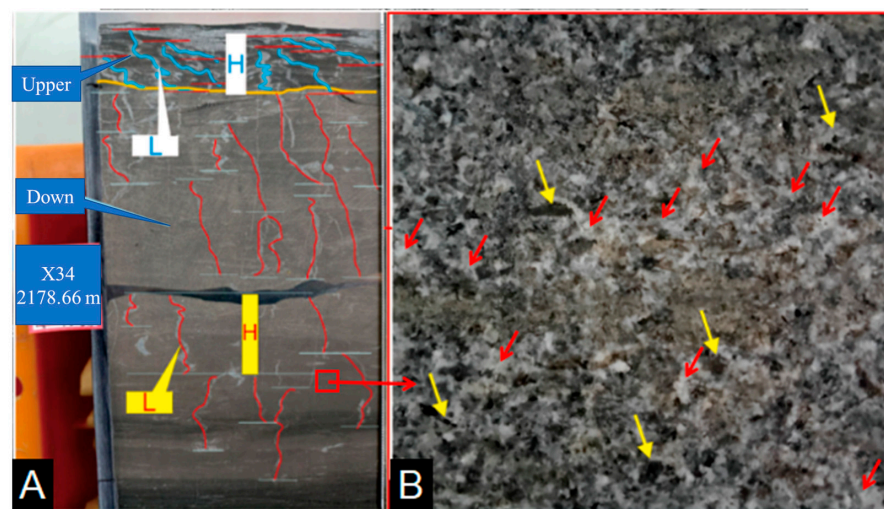


**Figure 16.** Silt veins in argillaceous dolomite. ((A). Silt veins in oil-bearing dolomite (red arrows) and in gray-black mud shale (blue arrows). Slightly curved silt veins in dolomite with a compaction ratio of 1.48 (Table 2) indicate trace compaction but no lateral shear. The silt veins in the top mud shale are clearly curved and inclined, with a compression rate of 2.68 (Table 3), H is the thickness of the rock, and L is the length of the sand veins. (B). Dolomite (nodules) with a large amount of grayish-brown chalk-grade mud flakes (yellow arrows) that account for approximately 40–50%, with dolomite between the mud flake particles; therefore, dolomite occurs as cement (red arrows), while dolomite (nodules) is just a layer of cloudy mudstone or muddy cloudstone.).

**Table 2.** Compaction rate of silt veins in dolomite.

Lower	Length (L)	Height (H)	L/H
1	12	9	1.333
2	13	9	1.444
3	14	6	2.333
4	8	5	1.600
5	31	15	2.067
6	19	14	1.357
7	32	28	1.143
8	13	8	1.625
9	7	5	1.400
10	35	26	1.346
11	38	28	1.357
12	64	49	1.306
13	24	19	1.263
14	18	15	1.200
15	34	26	1.308
16	13	9	1.444
17	12	8	1.500
18	8	6	1.333
19	35	23	1.522
20	26	14	1.857
21	16	14	1.143
22	24	13	1.846
23	16	12	1.333
24	28	15	1.867
25	14	12	1.167
26	13	8	1.625
27	12	9	1.333
28	16	11	1.455
29	13	9	1.444
Average	20.966	14.655	1.481

**Table 3.** Compaction rate of silt veins in mud shale.

Upper	Length (L)	Height (H)	L/H
1	8	5	1.600
2	13	8	1.625
3	21	10	2.100
4	10	6	1.667
5	21	4	5.250
6	24	5	4.800
7	19	11	1.727
8	14	5	2.800
9	22	12	1.833
10	14	5	2.800
11	33	10	3.300
Average	18.091	7.364	2.682

### 3.12. Study of Major Element Compositions in Dolomite Thin Layers and Nodules

The chemical analysis of dolomite nodules in the Gulong Qingshankou Formation shows the presence of SiO<sub>2</sub>, Al<sub>2</sub>O<sub>3</sub>, Fe<sub>2</sub>O<sub>3</sub>, and other minerals in addition to CaO and MgO (Table 4), indicating that dolomite from the Gulong Qingshankou Formation contains impurities, which is consistent with the results observed under electron microscopy. The chemical analysis of the thin-layer dolomite and dolomite nodules in the Qingshankou Formation in Gulong Sag shows that their chemical composition is discrete (Table 4) and is mainly composed of SiO<sub>2</sub>, Al<sub>2</sub>O<sub>3</sub>, Fe<sub>2</sub>O<sub>3</sub>, CaO, MgO, and Na<sub>2</sub>O. Pure white dolomite with more than 40% CaO and MgO is obtained. The content of CaO and MgO is between 30 and 40%, making it a clay-bearing dolomite. When the content of CaO and MgO is less than 30%, it is argillaceous dolomite (Table 4). This classification does not correspond exactly to the classification from mineralogy.

### 3.13. Carbon and Oxygen Isotope Characteristics

Carbon and oxygen isotopes of carbonate rocks are important in the study of carbonate rocks. Carbon and oxygen isotopes can further our understanding of the sedimentary environment and diagenetic process of carbonate rocks [4,12,13,31]. Carbon and oxygen isotopes are often used to discern the influence of (reservoir) magmatic hydrothermal action [32–36]. Carbon and oxygen isotope analyses were performed on the thin layers and nodules of dolomite (chert) in the Aoshankou Formation, and the results are summarized in Table 5. The distribution range of carbon isotopes ( $\delta^{13}\text{C}$ ) was 0.15 to 16.13‰, with an average of 7.18‰; the distribution range of oxygen isotopes ( $\delta^{18}\text{O}$ ) was −17.10 to −6.70‰, with an average of −11.09‰. The  $\delta^{18}\text{O}$  values of calcite veins in reservoirs subject to magmatic hydrothermal action in the Tarim range from −15.38‰ to −8.04‰ and are close to those of the shales of the Qingshankou Formation in Gulong Sag. Calcite  $\delta^{18}\text{O}$  values in the Bohai Bay Basin modified by hydrothermal fluids are significantly lower than −10‰, while these values in the unmodified hydrothermal fluids are greater than −10‰ [36]. This is also closer to the value in the shales of the Qingshankou Formation in Gulong Sag. The variation in  $\delta^{18}\text{O}$  values is primarily controlled by the nature of the medium and temperature, and the intrusion of hydrothermal fluids into the deep subsurface leads to an increase in the formation temperature and enhanced thermal fractionation, which in turn leads to low  $\delta^{18}\text{O}$  values of calcite modified by hydrothermal fluids [30]. The carbon and oxygen isotopes are shown in Figure 12, and they all fall in the magmatic hydrothermal zone, indicating that the dolomite of the Qingshankou Formation in the Gulong Sag was influenced by hydrothermal action. Moreover, it demonstrates that the Qingshankou Formation was influenced by magmatic hydrothermal action. The Oligocene lacustrine dolomites in the Yingxi area of Qaidam Basin were also subjected to magmatic hydrothermal transformation [10], and lacustrine hydrothermal sedimentary primary dolomite was also developed in the Cretaceous in Qingxi Sag of Jiuquan Basin along the northern margin of the Qinghai–Tibet Plateau [20].

**Table 4.** Chemical compositions of the thin dolomite layers and dolomite nodules of the Qingshankou Formation.

Sample	Depth (m)	Lithology	SiO <sub>2</sub>	Al <sub>2</sub> O <sub>3</sub>	Fe <sub>2</sub> O <sub>3</sub>	CaO	MgO	K <sub>2</sub> O	Na <sub>2</sub> O	TiO <sub>2</sub>	P <sub>2</sub> O <sub>5</sub>	MnO
A3-155	2174.17	Dolomite	5.61	2.23	7.39	29.72	13.36	0.44	0.29	0.11	0.14	0.38
A3-203	2227.04	Dolomite	19.87	17.94	4.01	31.2	12.01	3.67	1.56	0.6	0.08	0.05
A3-206	2229.58	Dolomite	19.76	18.73	4.41	30.53	11.87	3.77	1.63	0.65	0.1	0.03
A3-208	2230.89	Dolomite	18.66	18.48	4.43	30.86	11.85	3.78	1.62	0.64	0.16	0.05
A3-217	2238.29	Dolomite	15	17.76	4.88	32.51	12.89	3.69	1.24	0.59	0.14	0.06
A3-223	2242.09	Dolomite	19.06	17.68	4.45	30.69	11.96	3.23	1.87	0.6	0.11	0.03
A3-227	2245.36	Dolomite	2.34	1.26	5.84	28.62	17	0.23	0.18	0.06	0.26	0.16
A3-229	2247.04	Dolomite	9.18	3.12	6.92	25.73	14.61	0.18	0.18	0.08	0.15	0.14
A3-269	2275.36	Dolomite	7.31	1.35	3.21	31.13	14.89	0.16	0.15	0.04	0.14	0.28
A3-158	2177.36	Clay-bearing dolomite	8.1	2.89	9.78	27.63	12.07	0.4	0.34	0.1	0.19	0.28
A3-160	2179.8	Clay-bearing dolomite	15.33	2.26	7.18	25.82	12.07	0.22	0.44	0.08	0.21	0.21
A3-164	2181.93	Clay-bearing dolomite	20.23	6.43	8.04	21.67	9.17	1.2	1.04	0.26	1.4	0.29
A3-171	2189.7	Clay-bearing dolomite	16.82	2.93	8.82	24.83	11.32	0.31	0.35	0.09	0.22	0.29
A3-183	2206.17	Clay-bearing dolomite	19.89	3.86	7.46	23.61	10.36	0.64	0.5	0.13	0.44	0.28
A3-193	2216.01	Clay-bearing dolomite	15.87	4.87	8.13	23.78	11.12	0.91	0.46	0.18	0.19	0.32
A3-219	2239.58	Clay-bearing dolomite	23.44	4.66	8.25	19.89	11.15	0.33	0.24	0.1	0.05	0.21
A3-243	2256.85	Clay-bearing dolomite	24.12	5.3	7.64	20.61	9.75	0.93	0.32	0.18	0.12	0.25
A3-175	2195.59	Argillaceous dolomite	26.11	6.44	8.89	19.63	8.89	1.12	0.79	0.23	0.46	0.27
A3-197	2219.64	Argillaceous dolomite	37.6	12.16	6.93	11.29	6.84	2.37	1	0.43	0.13	0.14
A3-256	2265.97	Argillaceous dolomite	27.99	5.59	6.24	19.32	10.04	0.91	0.3	0.17	0.16	0.2
	Average		17.61	7.8	6.64	25.45	11.66	1.42	0.72	0.27	0.24	0.2

**Table 5.** Carbon and oxygen isotope analysis table of Guye 8 HC well and other wells.

Number	Sample Description	Horizon	Distance Top (m)	Well Depth (m)	Detection Result (%)		Paleosalinity (Z)	Paleowater Temperature (°C)	$\delta^{18}\text{O}_{\text{CaCO}_3}$ PDB
					$\delta^{13}\text{C}$ PDB	$\delta^{18}\text{O}$ PDB			
GY1-2	Gray micrite dolomite	K1qn1	21.40	2518.81	11.90	−6.49	144.60	3.39	3.40
GY1-3	Gray micrite dolomite	K1qn1	3.70	2527.72	2.18	−16.79	120.47	50.78	−6.90
GY1-4	Gray micrite dolomite	K1qn1	5.10	2529.12	0.28	−16.57	116.67	49.46	−6.68
GY1-5	Gray micrite dolomite	K1qn1	6.90	2530.92	1.67	−15.68	119.88	44.35	−5.79

Table 5. Cont.

Number	Sample Description	Horizon	Distance Top (m)	Well Depth (m)	Detection Result (%)		Paleosalinity (Z)	Paleowater Temperature (°C)	$\delta^{18}\text{O}_{\text{CaCO}_3}$ PDB
					$\delta^{13}\text{C}$ PDB	$\delta^{18}\text{O}$ PDB			
GY1-6	Gray micrite dolomite	K1qn1	8.30	2532.32	4.27	−14.71	125.61	38.98	−4.82
GY1-7	Gray micrite dolomite	K1qn1	10.40	2534.42	2.25	−16.49	120.74	48.97	−6.60
GY1-8	Gray micrite dolomite	K1qn1	11.30	2535.32	11.03	−8.88	141.83	11.94	1.01
GY1-9	Gray micrite dolomite	K1qn1	13.00	2537.02	9.53	−9.40	138.56	13.99	0.49
GY1-10	Gray micrite dolomite	K1qn1	16.20	2540.22	9.09	−9.46	137.63	14.21	0.43
GY1-11	Gray micrite dolomite	K1qn1	16.95	2540.97	4.86	−12.22	127.84	26.36	−2.33
GY1-12	Gray micrite dolomite	K1qn1	7.50	2551.16	10.41	−7.53	141.12	6.94	2.36
GY1-13	Gray micrite dolomite	K1qn1	9.50	2553.16	9.99	−7.89	140.11	8.22	2.00
GY1-15	Gray micrite dolomite	K1qn1	15.00	2558.66	9.27	−9.97	137.80	16.30	−0.08
GY1-16	Gray micrite dolomite	K1qn1	2.40	2575.00	9.29	−7.65	138.79	7.34	2.25
C9	Dolomite	K1qn1	0.90	2544.56	8.56	−9.06	136.70	12.64	0.83
GY2-1	Gray micrite dolomite	K1qn1	7.65	2286.94	3.52	−14.41	124.19	37.38	−4.52
GY2-2	Gray micrite dolomite	K1qn1	8.40	2287.69	6.11	−12.10	130.44	25.77	−2.21
GY2-3	Gray micrite dolomite	K1qn1	9.00	2288.29	7.03	−12.04	132.36	25.47	−2.15
GY2-4	Gray micrite dolomite	K1qn1	10.70	2289.99	12.23	−8.57	144.42	10.74	1.32
GY2-5	Gray micrite dolomite	K1qn1	11.60	2290.89	9.48	−10.12	138.16	16.94	−0.23
GY2-6	Gray micrite dolomite	K1qn1	13.00	2292.29	0.15	−16.72	116.35	50.33	−6.83
GY2-7	Gray micrite dolomite	K1qn1	13.70	2292.99	5.73	−13.34	129.17	31.82	−3.45

Table 5. Cont.

Number	Sample Description	Horizon	Distance Top (m)	Well Depth (m)	Detection Result (%)		Paleosalinity (Z)	Paleowater Temperature (°C)	$\delta^{18}\text{O}_{\text{CaCO}_3}$ PDB
					$\delta^{13}\text{C}$ PDB	$\delta^{18}\text{O}$ PDB			
GY2-8	Gray micrite dolomite	K1qn1	16.00	2295.29	7.09	−11.62	132.64	23.52	−1.73
GY2-9	Gray micrite dolomite	K1qn1	17.80	2297.09	3.59	−13.01	124.90	30.16	−3.12
GY2-10	Gray micrite dolomite	K1qn1	21.60	2300.89	2.48	−12.76	122.74	28.95	−2.87
GY2-11	Gray micrite dolomite	K1qn1	24.75	2304.04	12.83	−7.73	145.99	7.64	2.16
GY2-12	Gray micrite dolomite	K1qn1	4.80	2310.54	3.62	−13.47	124.78	32.45	−3.58
GY2-13	Gray micrite dolomite	K1qn1	5.20	2326.69	10.72	−9.12	141.12	12.87	0.77
GY2-15	Gray micrite dolomite	K1qn1	2.95	2333.61	7.52	−9.82	134.26	15.70	0.07
GY2-16	Gray micrite dolomite	K1qn1	3.90	2334.56	2.82	−12.52	123.54	27.79	−2.63
GY2-17	Gray micrite dolomite	K1qn1	1.50	2336.45	9.31	−8.71	138.38	11.28	1.18
GY2-18	Gray micrite dolomite	K1qn1	2.00	2336.95	8.63	−8.52	137.08	10.53	1.38
GY2-19	Gray micrite dolomite	K1qn1	3.56	2338.51	2.05	−14.94	120.97	40.24	−5.05
GY2-21	Gray micrite dolomite	K1qn1	0.80	2346.08	6.18	−11.21	130.94	21.69	−1.32
GY2-22	Gray micrite dolomite	K1qn1	2.50	2347.78	8.86	−9.82	137.01	15.69	0.07
GY2-23	Gray micrite dolomite	K1qn1	3.00	2348.28	3.90	−12.93	125.58	29.78	−3.04
GY2-24	Gray micrite dolomite	K1qn1	3.30	2348.58	3.83	−13.06	125.39	30.43	−3.17
GY2-25	Gray micrite dolomite	K1qn1	2.70	2353.11	4.65	−12.36	127.34	26.99	−2.47
GY2-26	Gray micrite dolomite	K1qn1	3.20	2353.61	5.06	−15.90	126.74	45.56	−6.01
GY2-27	Gray micrite dolomite	K1qn1	1.40	2356.49	12.70	−7.40	145.86	6.48	2.49

Table 5. Cont.

Number	Sample Description	Horizon	Distance Top (m)	Well Depth (m)	Detection Result (%)		Paleosalinity (Z)	Paleowater Temperature (°C)	$\delta^{18}\text{O}_{\text{CaCO}_3}$ PDB
					$\delta^{13}\text{C}$ PDB	$\delta^{18}\text{O}$ PDB			
GY2-28	Gray micrite dolomite	K1qn1	2.30	2357.39	13.08	−7.50	146.60	6.83	2.39
GY2-29	Gray micrite dolomite	K1qn1	0.10	2358.52	6.52	−11.53	131.52	23.11	−1.64
GY2-30	Gray micrite dolomite	K1qn1	0.90	2359.32	9.55	−10.43	138.16	18.27	−0.54
GY2-31	Gray micrite dolomite	K1qn1	11.80	2370.22	3.84	−14.63	124.75	38.52	−4.74
GY2-32	Gray micrite dolomite	K1qn1	13.10	2371.52	1.87	−17.10	119.72	52.61	−7.21
GY2-33	Gray micrite dolomite	K1qn1	13.50	2371.92	0.64	−16.53	117.43	49.25	−6.64
3	Gray dolomite	K1qn1	11.80	2370.22	7.37	−12.92	132.68	29.73	−3.03
C10	Dolomite	K1qn1	2.45	2357.54	14.43	−6.39	149.81	3.09	3.50
C11	Dolomite	K1qn1	7.15	2365.57	16.13	−8.67	152.38	11.11	1.22
C12	Dolomite	K1qn1	9.90	2494.20	7.43	−10.94	133.62	20.45	−1.05
C13	Dolomite	K1qn1	7.50	2491.80	6.69	−11.80	131.76	24.36	−1.91
11-2	Dolomitic mudstone	K2qn1	/	1746.44	11.16	−6.82	142.95	4.49	3.07
5-1	Dolomite	K1qn2+3	/	2115.80	8.33	−11.73	135.14	24.05	−1.84
B10-2	Dolomite	K2qn1	/	2369.78	8.28	−10.03	135.74	16.56	−0.14
B27-2	Dolomite	K2qn1	/	2350.70	5.53	−13.23	128.79	31.27	−3.34
B6	Dolomite	K2qn1	/	1665.22	16.78	−6.80	154.47	4.42	3.09
98B	Dolomitic mudstone	K2qn1	/	1060.22	2.06	−9.05	123.40	12.59	0.84
D9	Dolomite	K2qn1	/	2388.08	10.00	−8.05	140.07	8.80	1.84
1	Black dolomitic shale	K2qn1	/	2056.60	5.18	−11.98	128.59	25.21	−2.09
22	Dolomite	K2qn1	/	1994.05	9.97	−7.82	140.10	7.96	2.07
15	Gray dolomite	K2qn1	/	1870.14	11.34	−7.62	142.99	7.25	2.27
52	Gray dolomite	K2qn1	/	1826.93	5.97	−11.03	130.60	20.87	−1.14
B33	Dolomite	K2qn1	/	1596.72	5.27	−11.40	129.01	22.53	−1.51
99B	Dolomitic mudstone	K2qn1	/	1063.39	2.33	−9.28	123.86	13.50	0.61
416	Muddy dolomite	K2qn1	/	2522.68	12.48	−6.70	145.70	4.09	3.19
Average value					7.18	−11.09	133.05	22.32	−1.20

#### 4. Analysis of the Factors Underlying Dolomite Formation

From well Paleo 8HC, we can determine that the dolomite thin layers and nodules formed mainly in an arid climate. The high values of carbonate rocks correspond well with the high values of Sr/Cu, which correspond to an arid climate, and with the high values of Sr/Ba, which correspond to the degree of lake salinization. These findings reveal that dolomite was formed in an arid climate under lake salinization. Moreover, the dolomite layers correspond to oil shale and bottom tuff layers. Sr/Cu values greater than 10 correspond to an arid climate, and two Sr/Cu values greater than 210 were observed in well X 8HC (Table 3). The first value was found in section Q1 at the bottom of the Qingshankou Formation. The second value occurred between Q6 and Q7, corresponding to the demarcation line between Qing Sections 1 and 2 and a layer of tuff, thus revealing that a volcanic eruption and deep geological action occurred between Q6 and Q7 in Gulong Sag. In addition, approximately 10 areas with high Sr/Cu values were observed (Table 6), revealing a series of secondary drought events in addition to the two major drought events mentioned above. These values were nearly evenly distributed in the Qingshankou Formation, revealing that the drought events in the Qingshankou period occurred from the beginning to end. The high value of Sr/Ba almost strictly corresponds to Sr/Cu deposits, thus reflecting the salinization of the Gulong Sag through the Qingshankou period. During lake salinization, carbonate rocks are developed; therefore, from the dolomite development analysis, the Gulong Sag Qingshankou stage represents a (micro-)salinized environment. Other dolomite-producing lakes in China are also saline [9].

From the carbon and oxygen isotopes, the dolomite of the Qingshankou Formation in Gulong Sag was subjected to magmatic hydrothermal action; however, this action was superimposed on the sedimentary base. Therefore, the depositional environment of carbonate rocks is the main factor underlying the deposition of carbonate rocks. This depositional environment was primarily caused by the arid climate and lake salinization.

**Table 6.** Trace elements and paleoclimate and paleosalinity parameters in well SL 8 HC.

	Oil Layer	Ba (ppm)	Sr (ppm)	Cu (ppm)	Ni (ppm)	Cr (ppm)	V (ppm)	B (ppm)	Paleoclimate Sr/Cu (ppm)	Paleosalinity Sr/Ba (ppm)
X8HC	Q9	357.20–723.20 532.69 (17)	228.70–686.10 351.24 (17)	14.69–50.46 29.98 (17)	18.62–42.22 23.63 (17)	37.56–87.84 52.45 (17)	39.50–202.80 111.78 (17)	8.40–135.30 67.50 (17)	6.80–46.71 13.46 (17)	0.44–1.92 0.69 (17)
	Q8	398.40–1610.00 537.77 (16)	176.00–280.30 270.41 (16)	26.41–38.78 33.06 (16)	20.08–77.50 26.47 (16)	39.93–58.81 49.34 (16)	87.78–144.20 119.51 (16)	40.27–75.28 62.49 (16)	4.62–12.30 8.18 (16)	0.23–0.83 0.50 (16)
	Q7	244.80–566.80 414.10 (15)	197.50–557.20 303.30 (15)	23.20–42.75 33.56 (15)	18.58–32.76 25.04 (15)	31.92–59.84 47.90 (15)	80.71–148.20 118.35 (15)	40.81–92.92 65.59 (15)	4.96–23.17 9.04 (15)	0.45–2.09 0.73 (15)
	Q6	476.60–746.00 558.69 (15)	242.40–1194.00 449.01 (15)	5.53–39.54 29.66 (15)	5.60–32.88 24.82 (15)	12.37–63.56 48.89 (15)	26.28–131.30 102.22 (15)	13.51–87.75 71.53 (15)	6.87–210.16 15.14 (15)	0.48–1.79 0.80 (15)
	Q5	321.80–684.30 465.76 (9)	237.30–740.50 354.41 (9)	22.98–36.99 29.83 (9)	20.47–33.18 25.95 (9)	32.84–60.75 49.49 (9)	74.95–144.20 108.87 (9)	38.22–85.48 60.67 (9)	6.97–32.22 11.88 (9)	0.52–1.50 0.76 (9)
	Q4	310.30–498.30 424.01 (10)	182.70–999.70 321.20 (10)	17.36–40.00 30.81 (10)	18.30–25.03 23.48 (10)	33.41–62.61 50.14 (10)	87.73–146.70 121.06 (10)	43.87–66.66 57.96 (10)	6.24–57.59 10.43 (10)	0.42–2.01 0.76 (10)
	Q3	260.50–456.50 359.43 (13)	219.20–709.20 316.70 (13)	25.59–70.12 41.04 (13)	13.32–30.60 24.14 (13)	35.73–57.41 51.45 (13)	95.96–159.70 129.97 (13)	42.60–68.76 55.81 (13)	4.14–27.71 7.72 (13)	0.66–1.72 0.88 (13)
	Q2	303.00–364.40 343.03 (3)	248.30–358.70 300.73 (3)	33.42–40.06 36.01 (3)	24.43–31.06 28.36 (3)	46.53–54.24 50.95 (3)	120.10–130.10 125.30 (3)	41.83–52.54 46.85 (3)	7.19–10.73 8.35 (3)	0.81–0.99 0.88 (3)
	Q1	244.00–746.00 466.74 (11)	233.30–1162.00 418.72 (11)	5.53–39.84 29.03 (11)	5.60–29.87 23.43 (11)	12.37–55.93 43.62 (11)	26.28–134.90 102.63 (11)	13.51–87.75 61.04 (11)	6.02–210.16 14.42 (11)	0.51–2.09 0.90 (11)

## 5. Conclusions

The following conclusions were obtained:

- (1) A certain number of thin dolomite layers and nodules developed in the Gulong Shale oil reservoir and can be classified into three rock types: pure dolomite, with a dolomite or calcite content greater than 90%; mud-bearing dolomite, with a dolomite or calcite content 75–90%; and argillaceous dolomite, with a 50–75% dolomite or calcite content.
- (2) The thin dolomite layers and nodules developed silt veins, and the 1.48 compaction rate or curvature of the silt veins was smaller than that of the mud shale from this period, indicating that the thin dolomite layers and nodules were subjected to less compaction after they were formed. Therefore, dolomitization occurred soon after deposition.
- (3) The thin dolomite layers and nodules in the Gulong shale oil reservoir formed under arid climatic conditions because of the initial salinization of the Gulong Sag, and they were also subjected to magmatic hydrothermal action.
- (4) The thin layers and nodules of dolomite and in the Gulong shale oil reservoir also present a certain oil storage capacity. This characteristic determines the exploration and development potential of Gulong's shale oil, which has unique economic and technical attributes.

**Author Contributions:** G.S.: methodology, resources; W.D.: software, formal analysis, validation; X.Z.: methodology, writing—original draft; J.Z.: conceptualization, writing—review and original draft; N.S.: formal analysis. All authors have read and agreed to the published version of the manuscript.

**Funding:** This research was funded by National Natural Science Foundation of China, No. 42072138; 41572088.

**Data Availability Statement:** Data will be made available upon request.

**Acknowledgments:** We gratefully acknowledge the Research Institute of Exploration and Development, Daqing Oilfield Company Limited, for providing geological data and samples.

**Conflicts of Interest:** The authors declare no conflict of interest.

## References

1. Jin, Z.J.; Zhu, D.Y.; Hu, W.X.; Zhang, X.F.; Wang, Y.; Yan, X.B. Geological and Geochemical Signatures of Hydrothermal Activity and Their Influence on Carbonate Reservoir Beds in the Tarim Basin. *Acta Geol. Sin.* **2006**, *80*, 245–253.
2. Zou, C.N.; Zhang, G.S.; Yang, Z.; Tao, S.Z.; Hou, L.H.; Zhu, R.K.; Yuan, X.J.; Ran, Q.Q.; Li, D.H.; Wang, Z.P. Geological concepts, characteristics, resource potential and key techniques of unconventional hydrocarbon: On unconventional petroleum. *Pet. Explor. Dev.* **2013**, *40*, 385–454. [[CrossRef](#)]
3. Sun, H.Q. Exploration practice and cognitions of shale oil in Jiyang depression. *China Pet. Explor.* **2017**, *22*, 1–14.
4. Liu, W.; Wang, P. Genesis and environmental significance of the dolomite concretions from the Nenjiang Formation in the Songliao Basin, northeast ERN China. *Sediment. Facies Palaeogeogr.* **1997**, *17*, 22–26.
5. Kuang, L.; Tang, Y.; Lei, D.; Chang, Q.; Min, O.; Hou, L.; Liu, D. Formation conditions and exploration potential of tight oil in the Permian saline lacustrine dolomitic rock, Junggar Basin, NW China. *Pet. Explor. Dev.* **2012**, *39*, 657–667. [[CrossRef](#)]
6. Li, H.; Liu, Y.; Li, W.; Yang, R.; Lei, C.; Liu, L.Y.; Liu, H.F.; Li, H.P. The microbial precipitation of lacustrine dolomite from Permian formation, Urumchi, Xinjiang, China. *Geol. Bull. China* **2013**, *32*, 661–670.
7. Xiao, L. Sedimentary characteristics and control factors of lacustrine limestone of Nadu Formation of Paleogene in Nakun area of Baise. *J. Oil Gas Technol.* **2012**, *34*, 1–5.
8. Wen, H.; Zheng, R.; Qing, H.; Fan, M.; Li, Y.; Gong, B. Primary dolostone related to the Cretaceous lacustrine hydrothermal sedimentation in Qingxi Sag, Jiuquan Basin on the northern Tibetan Plateau. *Sci. China Ser. D Earth Sci.* **2014**, *44*, 591–604. [[CrossRef](#)]
9. Yuan, J.; Huang, C.; Cao, Z.; Li, Z.; Wan, C. Carbon and oxygen isotopic composition of saline lacustrine dolomite and its palaeoenvironmental significance: A case study of Lower Eocene Ganchaigou Formation in western Qaidam Basin. *Geochimica* **2015**, *44*, 254–266.
10. Zhang, H.; Chen, G.; Zhu, Y.S. Discovery and significance of dolomites altered by hydrothermal fluid in Oligocene reservoirs of the Yingxi area, Qaidam Basin. *Geol. Sci. Technol. Inf.* **2017**, *36*, 87–97.
11. Wang, G.; Cheng, R.; Wang, P.; Gao, Y.F. The forming mechanism of dolostone of Nenjiang Formation in Songliao Basin: Example from CCSD-SK II. *Acta Geol. Sin.* **2008**, *82*, 48–54.

12. Yan, G.; Liu, Z.; Song, H.; Han, X.; Zhang, Z.; Cheng, D. Genesis of the dolomite in the Shahejie Formation of JZ oilfield, Bohai Basin. *Mar. Geol. Front.* **2020**, *36*, 26–35.
13. Fu, X.; Meng, Q.A.; Wen, Z.; Bai, Y.; Gao, B.; Su, Y.X. Sedimentary Environment and Genetic Mechanism of Dolomites in the Qingshankou Formation, Songliao Basin. *Acta Sedimentol. Sin.* **2022**, *10*, 14027.
14. Chen, Z.; Chen, F. Kinematic characteristics of inversion structures in Songliao Basin. *J. Grad. School* **1996**, *10*, 390–396.
15. He, W.; Cui, B.; Wang, F.; Wang, Y.; Meng, Q.; Zhang, J.; Shao, H.; Wang, R.; Bai, Y.; Lin, X.; et al. Study on the shale fissures, shale calcite veins and oil-state of Qingshankou formation from Gulong Sag. *Geol. Rev.* **2022**, *68*, 693–741.
16. He, W.; Yun, J.; Zhong, J. Dolomitization making reservoirs and fissure-cave reservoirs of the Changxing formation in eastnorthern Sichuan. *Lithol. Res.* **2022**, *34*, 1–25.
17. Wang, G.; Wang, F.; Meng, Q.; Gu, S. Stratgic significance and research direction for Gulong shale oil. *Pet. Geol. Oilfield Dev. Daqing* **2020**, *39*, 8–19.
18. Sun, L. Shale oil in Gulong Sag. *Pet. Geol. Oilfield Dev. Daqing* **2020**, *39*, 1–7.
19. He, W.; Meng, Q.; Zhang, J. Controlling factors and their classification- evaluation of Gulong shale oil enrichment in Songliao Basin. *Pet. Geol. Oilfield Dev. Daqing* **2021**, *40*, 1–12.
20. He, W.; Meng, Q.; Feng, Z.; Zhang, J.; Wan, R. In-Situ accumulation theory and exploration and development practice of Gulong shale oil in Songliao Basin. *Acta Pet. Sin.* **2022**, *43*, 1–14.
21. He, W. Discovery of nm pores and nm fractures in Gulong shale oil reservoir and its significances. *Pet. Geol. Oilfield Dev. Daqing* **2022**, *41*, 1–15.
22. Shao, H.; Gao, B.; Pan, H.; Chen, G.; Li, L. Diagenesis-pore evolution for Gulong shale in Songliao Basin. *Pet. Geol. Oilfield Dev. Daqing* **2021**, *40*, 56–67.
23. Wang, F.; Fu, Z.; Wang, J.; Tang, Z.; Jiang, R. Characteristics and classiification of Gulong shale reservoir in Songliao Basin. *Pet. Geol. Oilfield Dev. Daqing* **2012**, *40*, 144–156.
24. Aigner, T. Storm deposits as a tool in facies analysis. In *Abstracts: International Association of Sedimentologists 1st European Meeting*; International Association of Sedimentologists: Bochum, Germany, 1980; p. 44.
25. Aigner, T. *Storm Depositional Systems*; Springer: Berlin, Germany, 1985; p. 119.
26. Aigner, T.A. *Storm Depositional Systems: Dynamic Stratigraphy in Modern and Ancient Shallow-Marine Sequences*; Lecture Notes in Earth Sciences; Springer: Berlin/Heidelberg, Germany, 1985; Volume 3, p. 174.
27. Myrow, P.M.; Lukens, C.; Lamb, M.P.; Houck, K.; Strauss, J. Dynamics of a Transgressive Prodeltaic System: Implications for Geography and Climate within a Pennsylvanian Intracratonic Basin, Colorado, U.S.A. *J. Sediment. Res.* **2008**, *78*, 512–528. [[CrossRef](#)]
28. Immenhauser, A. Estimating palaeo-water depth from the physical rock record. *Earth Sci. Rev.* **2009**, *96*, 107–139. [[CrossRef](#)]
29. Mohseni, H.; Al-Aasm, I.S. Tempestite deposits on a storminfluenced carbonate ramp: An example from the pabdeh formation (paleogene), zagros basin, Swiran. *J. Pet. Geol.* **2004**, *27*, 163–178. [[CrossRef](#)]
30. He, W.; Zhong, J.; Sun, N. Discovery and significance of tempestites and storm deposits in the Qingshankou Formation of the Gulong Sag, northeastern China. *Front. Earth Sci.* **2022**, *16648714*, 191.
31. Vasconcelos, C.; McKenzie, J.A.; Warthmann, R.; Bernasconi, S.M. Calibration of the  $\delta^{18}\text{O}$  paleothermometer for dolomite precipitated in microbial cultures and natural environments. *Geology* **2005**, *33*, 317–320. [[CrossRef](#)]
32. Ji, C.; Chen, C.; Wu, Z.; Yi, H.; Xia, G.; Zao, Z. Carbon and oxygen isotopes analysis of the fluid inclusions in Middle Jurassic saccharoidal dolostone of Qiangtang Basin and discussion on the genesis of dolostone. *Geol. Rev.* **2020**, *66*, 1186–1198.
33. Luczaj, J.A.; Harrison, W.B., III; Smith Williams, N. Fractured hydrothermal dolomite reservoirs in the Devonian Dundee Formation of the central Michigan Basin. *AAPG Bull.* **2006**, *90*, 1787–1801. [[CrossRef](#)]
34. Zhu, D.; Jin, Z.; Hu, W. Hydrothermal alteration dolomite reservoir in Tazhong area. *Acta Pet. Sin.* **2009**, *30*, 698–704.
35. Huang, S.J.; Lan, Y.F.; Huang, K.K.; Lü, J. Vug fillings and records of hydrothermal activity in the Middle Permian Qixia Formation, western Sichuan Basin. *Acta Petrol. Sin.* **2014**, *30*, 687–698.
36. Wang, K.; Hu, S.; Hu, Z.; Liu, W.; Huang, Q.; Shi, S.; Ma, K.; Li, M. Cambrian hydrothermal action in Gucheng area, Talimu Basin and its influences on reservoir development. *Acta Pet. Sin.* **2016**, *37*, 439–452.

**Disclaimer/Publisher’s Note:** The statements, opinions and data contained in all publications are solely those of the individual author(s) and contributor(s) and not of MDPI and/or the editor(s). MDPI and/or the editor(s) disclaim responsibility for any injury to people or property resulting from any ideas, methods, instructions or products referred to in the content.